Electromagnetic Control of Biological Assembly

Michael Benjamin Sano

Thesis submitted to the faculty of Virginia Polytechnic Institute and State University in partial fulfillment of the requirements for the degree of

Masters of Science
In
Engineering Mechanics

Rafael V. Davalos, Ph.D., Committee Chairman

Paul Gatenholm, Ph.D., Committee Member

Jake Socha, Ph.D. Committee Member

Keywords: *Acetobacter xylinum*, Biological assembly,
Directed biofabrication, Electrokinetics

April 23rd 2010 – ICTAS 310

Electromagnetic Control of Biological Assembly

Michael Benjamin Sano

Abstract

We have developed a new biofabrication process in which the precise control of bacterial motion is used to fabricate customizable networks of cellulose nanofibrils. This work describes how the motion of Acetobacter xylinum can be controlled by electric fields while the bacteria simultaneously produce nanocellulose, resulting in networks with aligned fibers. Since the electrolysis of water due to the application of electric fields produces the oxygen in the culture media far from the liquid-air boundary, aerobic cellulose production in 3D structures is readily achievable. Five separate sets of experiments were conducted to demonstrate the assembly of nanocellulose by Acetobacter xylinum in the presence of electric fields in micro and macro environments. This work demonstrates a new concept of bottom up material synthesis by control of a biological assembly process.

Acknowledgements

I would like to thank all of the colleagues, students, and professors who have helped bring this concept to fruition. I would like to thank Dr. Davalos and Dr. Gatenholm for their continued enthusiasm, encouragement, and support. I am deeply appreciative of all the members of the Bio-Electro-Mechanical Systems (BEMS) laboratory whose insight and intuition aided in the steady progression of this project. Additionally, I would like to thank my family, friends, and loved ones for their continuous support and encouragement. Without them, I surely would not be where I am today.

Contents

Chapter 1 Hypothesis:.....1

Chapter 2 Introduction.....1

Chapter 3 : Morphological Control.....13

4.1 Methods.....13

a. Bacteria Cellulose Synthesis.....13

b. Microfluidic Device Fabrication.....13

c. Microfluidic Device Cellulose Synthesis.....17

d. Fabrication of Micro-Growth Chambers for Cellulose Network Synthesis.....17

e. Micro–Growth Chamber Cellulose Production.....20

f. 15 mL Test Tube Cellulose Production.....21

g. 100 mL Beaker Cellulose Production.....21

h. 10mL OptiCell 1100 Cellulose Production.....21

4.2 Results.....22

a. Microfluidic Device Results.....22

b. Micro-Growth Chamber Results.....26

c. 15mL Test Tube Results.....29

d. 100mL Beaker Results.....30

e. 10mL Opticell 1100 Results.....30

f. Mechanical Testing Results.....31

Chapter 4 : Physical and Chemical Modification.....35

5.1 Introduction to Physical and Chemical Modification.....35

5.2 Methods of Physical and Chemical Modification.....36

5.3 Interesting Results.....37

a. Copper Nanowires.....37

b. Graphite Composite.....38

c. Platinum Coatings.....38

d. Phosphate Crystallization.....38

e. Resistor-Capacitor Circuit.....39

f. Sub-surface Cellulose Production 40
Chapter 5 : Future Work 41
6.1 Comprehensive Examination on the Effects of Electric Field Intensity 41
6.2 Comprehensive Mechanical Testing 41
6.3 Alternating Signals and Complex Network Morphologies 42
Chapter 6 : Conclusion 43
Chapter 7 : References ..... A

FIGURE 1: GRAM NEGATIVE *ACETOBACTER XYLINUM* EMBEDDED IN A CELLULOSE NETWORK. THIS BACTERIUM MEASURES APPROXIMATELY 2500NM IN LENGTH AND 650 NM IN WIDTH. 2
FIGURE 2: THE DENSE RANDOM CELLULOSE NETWORK PRODUCED BY *ACETOBACTER XYLINUM* 3
FIGURE 3: SCHEMATIC MODEL OF RIBBON ASSEMBLY IN A.XYLINUM. GLUCAN CHAINS ARE EXTRUDED FROM CELLULOSE SYNTHASE COMPLEXES RESIDING IN A LINEAR ROW ON THE SURFACE OF THE BACTERIA. (1). GLUCAN CHAINS FROM ONE ENZYME COMPLEX ARE ASSOCIATED BY VAN DER WAALS FORCES INTO A SUB-ELEMENTARY FIBRIL AND (2) ASSOCIATED WITH HYDROGEN BOUNDS INTO A MICROFIBRIL. IN THE LAST STEP THESE CRYSTALLINE MICROFIBRILS ASSOCIATE INTO A RIBBON APPROXIMATELY 100NM IN WIDTH (3). ADAPTED FROM HIRAI ET AL.[1] 4
FIGURE 4: SCHEMATIC DEPICTING THE FORCES ACTING ON A CELL UNDER A COULOMBIC FORCE. ALL FORCES ACT FROM THE CENTER OF THE CELL. 7
FIGURE 5: (A) SCHEMATIC OF THE FABRICATION PROCESS USED TO CREATE THE MICROFLUIDIC CHAMBERS. STEPS A THROUGH D ARE FOLLOWED ONLY ONCE TO CREATE A MASTER STAMP. STEPS E AND F ARE REPEATED TO PRODUCE AN INDEFINITE NUMBER OF EXPERIMENTAL DEVICES 14
FIGURE 6: (A) SEM IMAGE OF THE SILICON WAFER MOLD AT THE INTERSECTION BETWEEN THE SIDE AND THE MAIN CHANNEL OF THE MICROFLUIDIC DEVICE (B) SCALLOPING EFFECT AFTER DRIE (C) SURFACE ROUGHNESS OF THE WAFER AFTER GROWING AND REMOVING THE OXIDE LAYER. 15
FIGURE 7: MAGNIFIED VISUALIZATION OF THE DRIE SCALLOPING EFFECT 15
FIGURE 8: A) FABRICATION PROCESS FOR CREATING MICROFLUIDIC CHANNELS. B) SCHEMATIC SHOWING THE TOP VIEW OF THE CHANNELS WITH INSULATING PILLARS. C) EXPERIMENTAL SETUP FOR INTERFACING WITH MICROFLUIDIC CHANNELS. 1000UL PIPETTE TIPS ARE USED AS FLUID RESERVOIRS TO MAINTAIN PRESSURE EQUILIBRIUM ACROSS THE CHANNEL. D) TIME LAPSE IMAGES OF FLUORESCENTLY LABELED A. XYLINUM CELLS BEING CONTROLLED THROUGH THE MICROFLUIDIC CHANNEL BY ELECTROKINETIC AND DIELECTROPHORETIC FORCES. 17
FIGURE 9: SCHEMATIC OF THE SILICON ON GLASS STAMP USED TO CREATE MICRO-GROWTH CHAMBERS 19
FIGURE 10: SILICON STAMPS COVERED IN PDMS DURING THE STAMPING PROCESS. FOIL IS USED TO CREATE A MOULD, DISTRIBUTE HEAT, AND PREVENT PDMS FROM LEAKING 20
FIGURE 11: (A) A SINGLE A. XYLINUM CELL IS ENTANGLED IN THE DENSE RANDOM CELLULOSE NETWORK IT HELPED PRODUCE. (B) TWO A. XYLINUM CELLS EMBEDDED IN A CELLULOSE NETWORK UNDERGOING MITOSIS. (C) THE RANDOM NANOCELLULOSE NETWORK PRODUCED BY A. *XYLINUM*. 22
FIGURE 12: TIME LAPSE IMAGE OF CONTROLLED ELECTROKINETIC MOVEMENT OF *ACETOBACTER XYLINUM* A DISTANCE OF 200MM OVER 30 SECONDS WITH A 10V APPLIED ELECTRIC FIELD. CONTROL EXPERIMENTS HAVE NO NET MOVEMENT. 23
FIGURE 13: THE ELECTROKINETIC VELOCITY OF BACTERIAL CELLS (TOP) MEASURED FOR ELECTRIC FIELD STRENGTHS BETWEEN 2V/CM AND 30V/CM AND (BOTTOM) CALCULATED VELOCITY BASED ON ELECTROKINETIC MOBILITY. 23

Figure 14: Time lapse images of fluorescently labeled A. xylinum cells being moved through a microfluidic chamber by electrokinetic and dielectrophoretic forces. 24
Figure 15 Additional time lapse images of fluorescently labeled A. xylinum cells being moved through a microfluidic chamber by electrokinetic and dielectrophoretic forces 25
Figure 16: Acetobacter xylinum (A) driven through a micrifluidic channel by electrokinetic foces, (B) trapped by dielectrophoretic forces under the application of 400V/cm , and (C-D) selectivly released by turning off the electric field 25
Figure 17: SEM images of the cellulose networks produced under a) 0V/cm, b)0.15V/cm, c)0.303V/cm, d)0.45V/cm at 5000x magnification 26
Figure 18: Cellulose network produced under a 0.303V/cm electric field at (a) 500x (a), (b) 2000x (b) and (c) 5000x (c) magnification. 28
Figure 19: Cellulose network produced under a 0.45V/cm electric field at (a) 2500x, (b) 1344x and (c) 4000x magnification 28
Figure 20: Cellulose growth in multiple layers by adding small quantities of culture media at discrete time points. 29
Figure 21: BC Production after 20 minutes in a 100mL beaker w/ 10V applied by aluminum electrodes. (a) Top view. (b) Fibers stained with calcoflour white and imaged with fluorescent microscopy. 30
Figure 22 : Fibers stretching across OptiCell culture platform produced by the application of 0.31V/cm (2.0V) 31
Figure 23: Instron Tensile testing system used to measure the mechanical properties of cellulose networks. 32
Figure 24: Failure of a cellulose network at the grippers under tensile load 33
Figure 25: Typical tensile testing results from samples prepared at 2, 4.5, and 5V in a 4.5cm micro-chamber. 34
Figure 26: Young's Modulus of samples grown in a 4.5x0.5 cm micro-chamber. 35
Figure 27: Schematic of the hypothesized process for ion deposition onto a cellulose nano-fiber 36
Figure 28: Copper coated cellulose network produced under the influence of a 1V/cm (1.5V) electric field 37
Figure 29: An individual cellulose fiber surrounded by copper ions forming an interconnected network. 37
Figure 30: An individual cellulose fiber surrounded by copper ions forming an interconnected network. 37
Figure 31: Platinum deposited onto a cellulose network cultured under the influence of a 0.15V/cm (0.25V) electric field 38
Figure 32: Elemental detection results for the cellulose network produced in a 25% PBS culture media under the application of 0.44V/cm (2V) by aluminum electrodes shows an increased presence of phosphorous and aluminum. 38
Figure 33: Phosphorous deposited onto a cellulose network cultured under the influence of a 0.44V/cm (2.0V) electric field 38
Figure 34: Schematic of the resistor-capacitor microfluidic channel pair. 39
Figure 35: Composite image of the resistive leg after 48 hours of cultivation showing the progression of metallization through the channel. 39
Figure 36: The resulting cellulose network after 96 hours of cultivation under 0.152V/cm (1.35V) applied by aluminum electrodes 39
Figure 37: Cellulose production below the liquid-air interface after 8 hours under the application of 16V in test tubes containing tap water (left) and tap water with methylene blue(right). 40
Figure 38: Cellulose production below the liquid-air interface observed when the applied voltage reaches 1.0V. 40
Figure 39: Schematic electrode activation pattern to produce zig-zag patterned nano-cellulose 42
Figure 40: Schematic of a nano-structure which will result in a negative Young's modulus. A material with this structure will expand in all directions when pulled in one direction. 42

Chapter 1 : **Hypothesis**

Electromagnetic fields can be used to manipulate the morphology and physical characteristics of a biologically assembled polymer.

Chapter 2 : **Introduction**

Biological systems such as microbes, animals, and plants produce complex hierarchal structures with precision spanning many length scales. Traditional manufacturing methods for small-scale devices, such as microfabrication, have limitations with regard to control of shape and size. Since top-down manufacturing methods are inadequate for manufacturing larger devices with complex nano-sized features, there is an emerging interest in using biological systems for bottom-up manufacturing. Biofabrication, the combination of biology and microfabrication, may be the future solution for the production of complex 3D architectures with nanoscale precision[2]. Such processes are advantageous since many organisms are preprogrammed to fabricate complex structures.

Our strategy to control these biofabrication processes is to interact with biological systems using various electro-magnetic stimuli. It has been previously demonstrated that bacteria can be magnetically manipulated to create complex magnetite nanoparticle chains[3] or be ultrasonically processed to create hollow metal chalcogenide nanostructures[4], and genetically engineered viruses can be used to fabricate ordered arrays of quantum dots[5]. A vast number of other potentially useful biological processes exist, and biological assembly can be affected by various stimuli such as electrical fields, magnetic fields, temperature, pH, or chemical gradients.

Researchers have previously demonstrated the use of electromagnetic fields to manipulate particles. For example, dielectrophoresis, the motion of a particle due to its polarization induced by a non-uniform electric field, has been used extensively to selectively concentrate cells and particles [6-11]. Magnetophoresis, the force exerted on a particle in an inhomogeneous magnetic field, has been used in field-flow fractionation [12-15] to alter the path of cells in microfluidic channels. The combination of electric and magnetic fields has been used in electromagnetophoresis, the migration of a cell in electrolyte solution in the direction perpendicular to both a magnetic field and an electric current[16], to separate biological samples [17, 18]. The effects of these electromagnetic fields on the viability of bacterial cells have been studied and it has been found that at low levels (1mT and less), cellular DNA fingerprints[19] and morphology[20] are not altered.

Here I present a method of direct control over bacterial cellulose nanofiber orientation using electrokinetic forces. We hypothesized that Acetobacter xylinum could be directed using electric fields while they produced nanocellulose fibers. We verified our hypothesis through four separate sets of experiments in micro and macro environments. Micro-scale experiments were conducted in custom

fabricated polymeric micro-chambers using simple stamping techniques. The macro-scale experiments were conducted in readily available laboratory supplies such as test tubes, beakers, and cell culture platforms. This paper is the first to describe electromagnetic control of bacteria during nanocellulose production. There are numerous other microbial species which complete precise biofabrication processes and these results suggest that similar techniques can be used to create materials with distinct properties which are not achievable using traditional manufacturing methods.

Introduction to Acetobacter xylinum

Cellulose, a natural polymer produced by the majority of plants, can also be assembled into nanofibrils by bacteria [21]. Acetobacter xylinum is a non-pathogenic, gram negative, cellulose producing bacterium which measures approximately 2.5μm in length and 650nm in width (Figure 1). Cellulose synthesis by Acetobacter xylinum is a rather complex process which involves the polymerization of single glucose molecules into β-1→4-glucan chains, the extracellular "extrusion" of the linear chains, and the assembly of the cellulose chains into ribbon-like fibrils with typical dimensions on the nanometer scale [22]. As a result of the motion of these bacteria, a three-dimensional network of randomly organized fibers is produced. The water binding ability of these cellulose ribbons, due to their large surface area and high concentration of hydrophilic hydroxyl groups, yields a hydrogel-like material with unique mechanical properties[23]. This cellulose network is particularly viable as a material for biomedical applications due to its' high purity, biocompatibility, mechanical integrity, hydroexpansivity, and its stability under a wide range of conditions[24]. Bacterial cellulose has been successfully evaluated in several biomedical applications including blood vessel replacement, meniscus, and as scaffolds for bone regeneration [25-27].

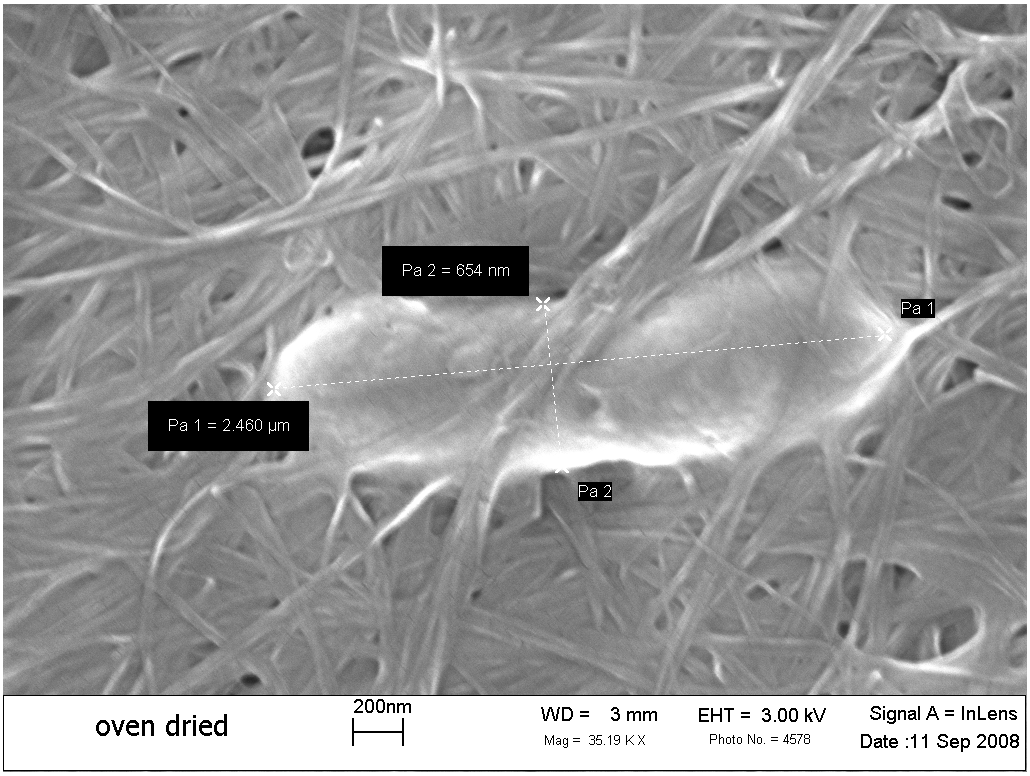

Figure 1: Gram negative *Acetobacter xylinum* embedded in a cellulose network. This bacterium measures approximately 2500nm in length and 650 nm in width.

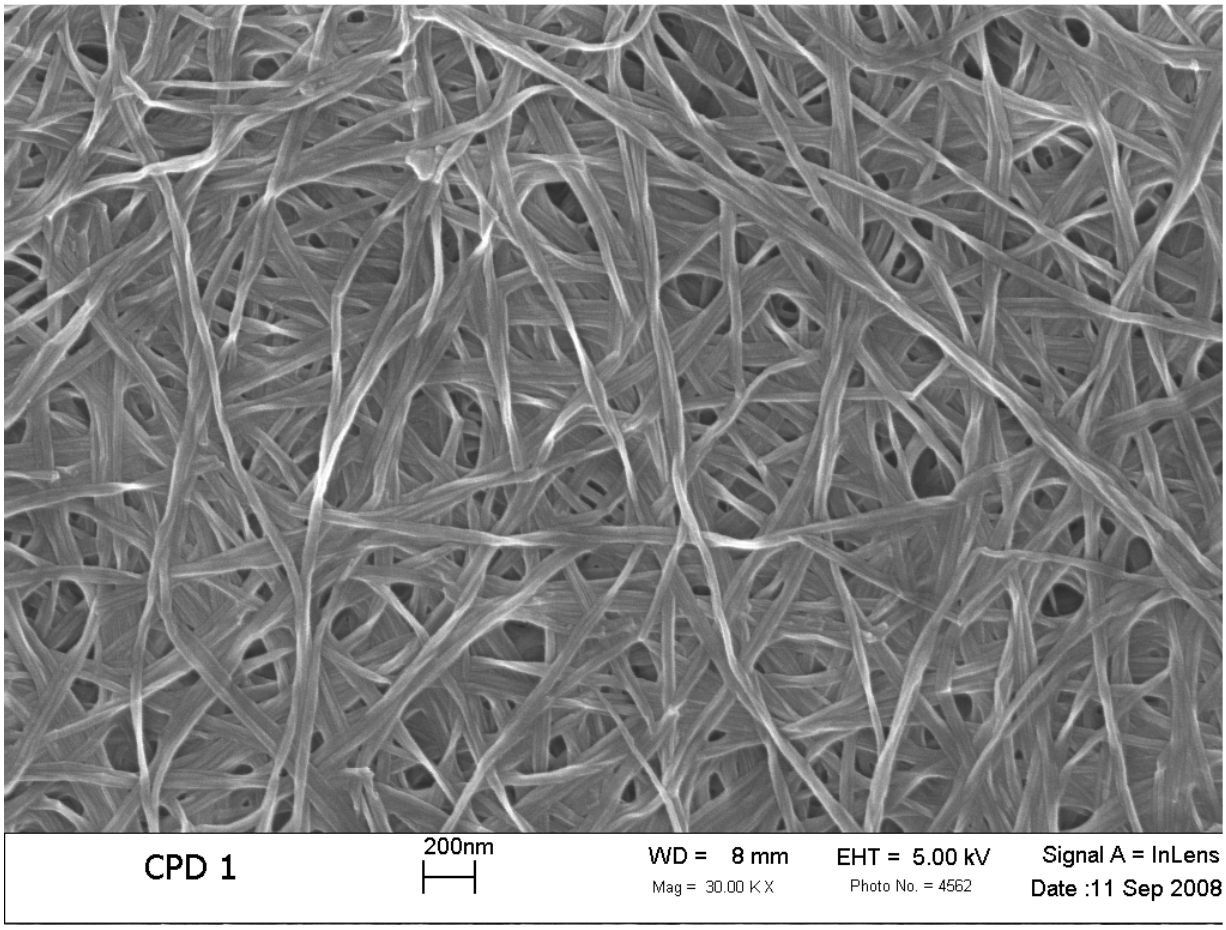

Figure 2: The dense random cellulose network produced by *Acetobacter xylinum*

The synthesis of cellulose in Acetobacter xylinum takes place between the outer and cytoplasma membrane. Cellulose is a product of carbon metabolism and, depending on the physiological state of the cell, involves either the pentose phosphate cycle or the Krebs cycle coupled with glucogenesis. The growing glucan chains are believed to aggregate and are exported through catalytic sites that are linearly arranged on each cell. Acetobacter xylinum assembles glucan chains into microfibrils and subsequently into a ribbon configuration as seen in Figure 3.

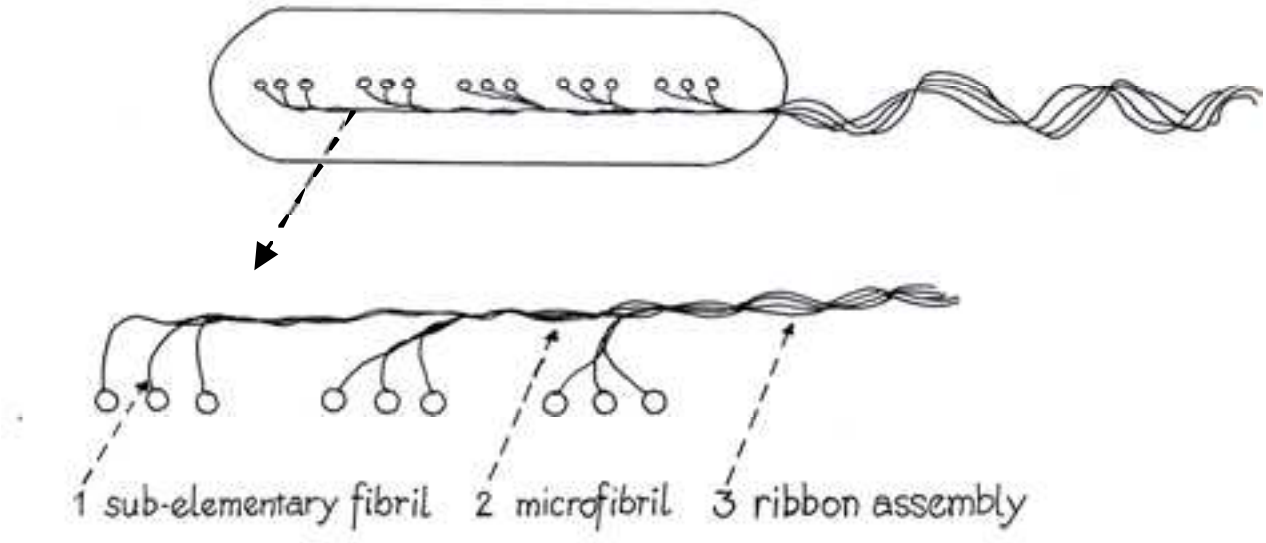

Figure 3: Schematic model of ribbon assembly in A.xylinum. Glucan chains are extruded from cellulose synthase complexes residing in a linear row on the surface of the bacteria. (1). Glucan chains from one enzyme complex are associated by van der Waals forces into a sub-elementary fibril and (2) associated with hydrogen bounds into a microfibril. In the last step these crystalline microfibrils associate into a ribbon approximately 100nm in width (3). Adapted from Hirai et al.[1]

Previous investigators have made steps towards overcoming this limitation by manipulating the shape and morphology of bacterial cellulose material by delivering oxygen to the culture media through a polymeric interface[28]. Other groups such as Putra et al. found that A. xylinum grown on permeable polydimethylsiloxane (PDMS) substrate showed birefringence indicating some degree of uniaxial fiber alignment [29]. They have also found that bacterial cellulose tubes grown on silicone tubing showed nanofiber orientation along the longitudinal axis [30]. Uraki et al. were able to align cellulose nanofibers along honeycomb-patterned microgrooves in an agarose film scaffold[31]. Kondo et al. found that bacterial cellulose grown on a molecular substrate of aligned glucan chains resulted in epitaxial aligned bacterial cellulose nanofibers [32]. While these modifications are limited to the fibrils located near the solid-liquid interface, these researchers shed light on the need for controlled orientation of the nanofibers.

Introduction to Electromagnetic Forces Acting on Particles in a Microfluidic Context

The application of a uniform electric field to an ionic liquid in a microfluidic field gives rise to electrical double layer (EDL) formation along the channel wall. The ions closest to the channel walls are subject to strong electrostatic forces which cannot be overcome by thermal diffusion. As result, these ions are statically bound to the surface of the channel forming a fixed Stern layer. The electrostatic force within the EDL deteriorates further from the channel surface and mobile ions begin to move parallel to the

EDL. The net effect of ionic drag caused by the mobile ions on the bulk fluid induces a phenomenon known as *electro-osmotic(EO) flow*.[33] The velocity of an ionic fluid under EO flow (v_{eo}) is calculated by [33]

$$v_{eo} = \mu_{eo}\vec{E} \qquad 1.$$

where μ_{eo} is the elctro-osmotic mobility of the ionic fluid and $\vec{E}$ is the magnitude of the applied electric field. The electro-osmotic mobility

$$\mu_{eo} = -\frac{\epsilon\zeta}{\eta} \qquad 2.$$

is a function of the surface potential between the solid and liquid phase (ζ) and the viscosity (η) of the fluid [34].

An EDL will additionally form around a charged particle (or cell) placed in an infinite ionic liquid under a uniform field. In the case of a positively charged cell, a double layer consisting of an excess of positive ions will form. The cell will then be driven towards the region of highest positive potential by a Coulombic force ($\vec{F_c}$) which is proportional to the net charge of the cell (q) and equal to

$$\vec{F_c} = q\vec{E} \qquad 3.$$

[35]. This force is also known as *electrophoresis* and the resulting electrophoretic velocity ($\vec{V}_{ep}$) of a spherical cell can be calculated using the Hückel equation[34]

$$\vec{V}_{ep} = \mu_{ep}\vec{E} \qquad 4.$$

This velocity is a function of the electrophoretic mobility (μ_{ep}) of the cell and the applied field. The electrophoretic mobility

$$\mu_{ep} = \frac{V_{ep}}{E} = \frac{q}{f} \qquad 5.$$

$$f = 6\pi\mu a \; is \; the \; stokes \; frictional \; factor \; for \; a \; spherical \; particle \; in \; creeping \; flow$$

$$\mu_{ep} = -\frac{3}{2}\frac{\epsilon_m\zeta_p}{\mu} \qquad 6.$$

is a function of the surface potential between the cell and the surrounding medium (ζ_p) and the permittivity of the surrounding media (ϵ_m). The net velocity of the cell as result of these two forces is referred to as the *electrokinetic velocity* ($\vec{V}_{ek}$)

$$\vec{V}_{ek} = (\mu_{eo} + \mu_{ep})\vec{E} \qquad 7.$$

where μ_{eo} and μ_{ek} are the electro-osmotic and electrophoretic mobilities respectively. These two terms summed are often referred to as the electrokinetic mobility of a particle (μ_{ek}).

$$\vec{V}_{ek} = \mu_{ek}\vec{E} \qquad 8.$$

A charged particle (or cell) placed in an infinite ionic liquid under a nonuniform field will become polarized and develop a charge distribution across the volume of the particle. The cell will then be driven towards the regions of maximal field gradient by a translational *dielectrophoretic* force ($\vec{F}_{DEP}$) [36]

$$F_{DEP} = \mu_{DEP} \cdot \nabla \mathrm{E} \qquad 9.$$

where μ_{DEP} is the dielectrophoretic mobility, or induced dipole moment, of the cell. For a bacterial cell with a round cylindrical shape in a non-uniform DC electric field, μ_{DEP} can be approximated as

$$\mu_{DEP} = v\vec{P} \qquad 10.$$

$$v = v_{cyl} + v_{cir} = \pi r^2 h + \frac{4}{3}\pi r^3 = \pi r^2 (h + \frac{4}{3} r) \qquad 11.$$

$$\vec{P} = (K_2 - K_1)(\frac{3K_1}{K_2 + 2K_1})\epsilon_0\vec{E} \qquad 12.$$

where v is the volume of an *A. xylinum* cell and $\vec{P}$ is the moment per unit volume with K1 and K2 are the relative dielectric constants of the liquid and the cell respectively.

$$\mu_{DEP} = \pi \mathrm{r}^2(\mathrm{h} + \frac{4}{3}\mathrm{r})(K_2 - K_1)(\frac{3K_1}{K_2 + 2K_1})\epsilon_0\vec{E} \qquad 13.$$

The net dielectrophoretic force becomes

$$F_{DEP} = \pi \mathrm{r}^2(3\mathrm{h} + 4\mathrm{r})\frac{K_1(K_2 - K_1)}{K_2 + 2K_1}\epsilon\nabla\overrightarrow{E^2} \qquad 14.$$

In an alternating (AC), non-uniform, electric field, the effects of frequency on the magnitude and sign of the dielectric constants of the particle and suspending medium must be considered when calculating the moment per unit volume ($\vec{P}$).

$$\vec{P} = 4\pi\epsilon_m K(\omega) r^3 \vec{E} \qquad 15.$$

K(ω) is the Clausius - Mossotti factor

$$K(\omega) = \frac{\epsilon_p^* - \epsilon_m^*}{\epsilon_p^* + 2\epsilon_m^*} \qquad 16.$$

$$\epsilon^* = \epsilon + \frac{i\sigma}{\omega}$$

where ω is the angular frequency of the applied field, ϵ is the permittivity, σ is the conductivity, and the subscripts $_p$ and $_m$ denote the properties of the particle and the surrounding medium respectively. The resulting dielectrophoretic force is

17.

In the case of cells, which exist in a micron scaled regime, these forces are opposed by a Stokes drag force.

18.

where is the mass density of the fluid, is the velocity of the cell relative to the fluid. The velocity of the particle can then be calculated by evaluating the balance of forces.

19.

Rearranging these terms:

20.

The term —— is known as the characteristic time and for cells in a microfluidic environment, is on the order of . The acceleration term in this equation is assumed to be zero since the characteristic time for small particles is orders of magnitude smaller than the time scale of external forces. From this the velocity of a particle can be calculated as follows:

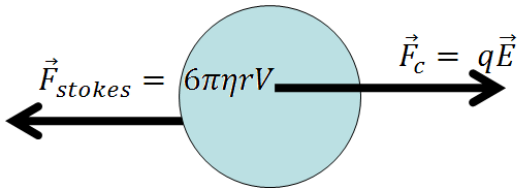

Figure 4: Schematic depicting the forces acting on a cell under a Coulombic force. All forces act from the center of the cell.

21.

The term $\mu_{DEP}$is known as the dielectrophoretic mobility. When cells encounter a region in which electrokinetic forces and dielectrophoretic forces are equal and critically oppose each other, the cells net velocity is reduced and they become trapped. For small velocities, the drag forces acting on a cell can be neglected and the net forces acting on a cell can be represented by

$$\mu_{ek}\vec{E} + \mu_{DEP}\nabla\left(\vec{E} \circ \vec{E}\right) = 0 \qquad 22.$$

In general, the value $\nabla\left(\vec{E} \circ \vec{E}\right)$ is difficult to calculate analytically and is typically approximated via computational simulation. Additionally, μ_{ek} can be analytically calculated if K1 and K2 are known, or as done in this study, it can be quantitatively measured via simple experimentation. From this, the dielectrophoretic mobility of a cell can be approximated by

$$\mu_{DEP} \approx \left|\frac{\mu_{ek}\vec{E}}{\nabla\left(\vec{E} \circ \vec{E}\right)}\right| \qquad 23.$$

A similar phenomenon, magnetophoresis, is observed for particles immersed in an inhomogeneous magnetic field. Magnetic field strength (**H**) is defined as

$$M_{ij} = \chi H_{ij} \qquad 24.$$

where χ is the magnetic susceptibility of a linear isotropic material and **M** is the magnetic dipole moment. In the absence of an externally applied **H** field, the internal magnetic field (magnetic flux density) **B** is

$$B_{ij} = \mu_0 M_{ij} \qquad 25.$$

where $\mu_0$is the permeability of free space. In the presence of an external H field, the internal magnetic field becomes

$$B_{ij} = \mu_0 M_{ij} + \mu_0 H_{ij} \qquad 26.$$

and combining the two previous equations yields the relationship between an internal magnetic field and the externally applied magnetic field.

$$B_{ij} = \mu_0 \chi H_{ij} + \mu_0 H_{ij} \qquad 27.$$
$$B_{ij} = \mu_0 (1 + \chi) H_{ij}$$

Maxwell's Equations for magnetostatics state that

$$\nabla \cdot \mathbf{B} = 0 \qquad 28.$$

$$\nabla \times \mathbf{H} = \mathbf{J} \qquad 29.$$

where **J** is the current density per unit area.

To establish a relationship between an applied electric field and the resultant magnetic field, first consider **E**, a conservative matrix which can be expressed as

$$\mathrm{E_{ij}} = -\nabla \mathrm{V} \tag{30.}$$

where V is a scalar quantity representing an applied voltage.

$$\nabla \times E_{ij} = -\frac{\delta}{\delta t}(\nabla \times A_{ij}) \tag{31.}$$

where **A** is any arbitrary matrix that satisfies $\nabla \times \mathrm{A_{ij}} = 0$. Switching to Einstein notation, this expression can be evaluated as follows:

$$\begin{aligned}
&e_i \frac{\delta}{\delta x_i} \times E_{jk} e_j \otimes e_k = -\frac{\delta}{\delta t}\left(e_i \frac{\delta}{\delta x_i} \times A_{jk} e_j \otimes e_k\right) \qquad 32.\\
&\mathrm{E_{jk,i}e_i \times (e_j \otimes e_k)} = -\dot{\overline{A_{jk,l}}} e_i \times (e_j \otimes e_k)\\
&E_{jk,i}(e_i \times e_j) \otimes e_k = -\dot{\overline{A_{jk,l}}}(e_i \times e_j) \otimes e_k\\
&E_{jk,i}(\mathrm{\epsilon_{ijl}e_l}) \otimes e_k = -\dot{\overline{A_{jk,l}}}(\epsilon_{ijl} e_l) \otimes e_k\\
&\epsilon_{ijl} E_{jk,l} e_l \otimes e_k = -\epsilon_{ijl}\dot{\overline{A_{jk,l}}}\, e_l \otimes e_k
\end{aligned}$$

Then, setting this equal to zero:

$$\begin{aligned}
&\epsilon_{ijl} E_{jk,l}\, e_l \otimes e_k + \epsilon_{ijl}\dot{\overline{A_{jk}}}_{,l}\, e_l \otimes e_k = 0 \qquad 33.\\
&(\epsilon_{ijl} E_{jk,l} + \epsilon_{ijl}\dot{\overline{A_{jk}}}_{,i})\, e_l \otimes e_k = 0\\
&\epsilon_{ijl}\left(E_{jk,l} + \dot{\overline{A_{jk}}}_{,i}\right) e_l \otimes e_k = 0\\
&\epsilon_{ijl}\left(E_{jk} + \dot{\overline{A_{jk}}}\right)_{,l}\, e_l \otimes e_k = 0
\end{aligned}$$

If we assume $\left(E_{jk} + \dot{A_{jk}}\right) = \tilde{E}_{jk}$ to be conservative then

$$\begin{aligned}
&\tilde{E}_{jk} = -\nabla \mathrm{V} \qquad 34.\\
&\left(E_{jk} + \dot{A_{jk}}\right) = -\nabla V\\
&E_{jk} = -\nabla V - \dot{A_{jk}}
\end{aligned}$$

Now taking the curl of both sides

$$\frac{\delta}{\delta_k} e_k \times [\, E_{ij}\, e_i \otimes e_j = -V_{,i} e_i - \dot{A_{\imath j}} e_i \otimes e_j] \tag{35.}$$

$$\nabla \times \boldsymbol{E} = \frac{\delta}{\delta_k} e_k \times V_{,i} e_i - \frac{\delta}{\delta_k} e_k \times \dot{A_{ij}} e_i \otimes e_j$$
$$\nabla \times \boldsymbol{E} = \frac{\delta}{\delta_k} V_{,i}\, e_k \times e_i - \frac{\delta}{\delta_k} \dot{A_{ij}} (e_k \times e_i) \otimes e_j$$
$$\nabla \times \boldsymbol{E} = \epsilon_{ikl} V_{,ik} e_l - \epsilon_{ikl}\, \overline{\dot{A}_{ij}}, k\ e_k \otimes e_j$$

Note that $\epsilon_{ikl} V_{,ik}$ violates the definition of a symmetric/antisymmetric tensor and must be zero resulting in

$$\nabla \times \boldsymbol{E} = -\epsilon_{ikl}\, \overline{\dot{A}_{ij}}, k e_k \otimes e_j \qquad 36.$$
$$\nabla \times \boldsymbol{E} = -\overline{\dot{\nabla \times \boldsymbol{A}}}$$
$$\nabla \times \boldsymbol{E} = -\dot{\boldsymbol{B}}$$

which is Maxwell's relation for electro-magnetic fields. Under the influence of a magnetic field, a particle will develop a magnetic potential energy (U)

$$U = \frac{(\chi_p - \chi_m)}{2\mu_0} V B^2 \qquad 37.$$

Where χ_p and χ_m are the volume magnetic susceptibility of the particle and media respectively, V is the volume of the particle, μ_0 is the magnetic permeability of a vacuum, and B is the magnetic flux density. A force equivalent to the gradient of the magnetic potential energy, magnetophoretic force (F_{MP}), is exerted on the particle such that

$$F_{MP} = -\nabla \mathrm{U} = \frac{\chi_\mathrm{p} - \chi_\mathrm{m}}{2\,\mu_0} V (\boldsymbol{B} \cdot \boldsymbol{\nabla}) \cdot \boldsymbol{B} \qquad 38.$$

In a microfluidic context, a spherical particle will also experience a Stokes drag force:

$$F_{Drag} = 6\pi\eta r v \qquad 39.$$

where η is the dynamic viscosity of the fluid, r is the radius of the particle, and v is the instantaneous velocity of the particle. The velocity of the particle can then be calculated by evaluating the balance of forces.

$$F_{MP} - F_{Drag} = m * a \qquad 40.$$

The acceleration term in this equation is assumed to be zero since the characteristic time for small particles is orders of magnitude smaller than the time scale of external forces. From this the velocity of a particle can be calculated as follows:

$$F_{MP} = F_{Drag} \qquad 41.$$
$$2[\chi_p - \chi_m]\left[\frac{4}{3}\right]\pi r^3 (B \cdot \nabla) \cdot B = 6\pi\eta r v$$

$$v = \frac{2(\chi_p - \chi_m)\left[\frac{4}{3}\right]\pi r^3}{6\pi\eta r}(B \cdot \nabla) \cdot B$$

$$v = \frac{2(\chi_p - \chi_m)\pi r^2}{9\mu_0\pi\eta}(B \cdot \nabla) \cdot B$$

Introduction to Tissue Engineering

Tissue engineering holds great promise for treating some of the most devastating diseases of our time. Because engineered tissue and organ replacements can be developed in a laboratory, therapies can potentially be delivered on a large scale, for multiple disease states with dramatic reduction in waiting times for patients. The concept of engineering tissue using selective cell transplantation has been applied experimentally and clinically for a variety of disorders, including the successful use of engineered bladder tissue for bladder reconstruction[37], engineered injectable chondrocytes for the treatment of vesicoureteral reflux[38] and urinary incontinence[39].

For clinical use, the process involves the seeding and attachment of human cells onto a scaffold[40]. Once seeded, the cells proliferate, migrate into the scaffold, and differentiate into the appropriate cell type for the specific tissue of interest while secreting the extracellular matrix components required to create the tissue. The three dimensional structure of the scaffold, and in particular the size of pores and density of the scaffold, is important in successful proliferation and migration of seeded cells to create the tissue. Therefore, the choice of scaffold is paramount in enabling the cells to behave in the required manner to produce tissues and organs of the desired shape and size.

Scaffolds for tissue engineering usually consist of polymers, both natural and synthetic. Some methods of forming scaffolds for tissue engineering from polymers are solvent-casting particulate-leaching, gas foaming of polymers[41], phase separation[42], and solution casting[43]. Electrospinning is another popular method for creating scaffolds for engineered tissues and organs but the technique suffers from fundamental manufacturing limitations that have to date prevented its clinical translation[44]. These limitations result from the distinct lack of processes capable of creating electrospun structures on the nano-, micro-, and millimeter scales that adequately promote cell growth and function.

The most successful scaffolds used in both pre-clinical animal studies and in human clinical applications are biological (natural) and made by decellularizing organs of large animals (e.g., pigs). In general, removal of cells from a tissue or an organ for preparation of a scaffold should leave the complex mixture of structural and functional proteins that constitute the extracellular matrix (ECM). The tissues from which the ECM is harvested, the species of origin, the decellularization methods and the methods of terminal sterilization for these biologic scaffolds vary widely. However, the decellularization methods are relatively harsh and result in significant destruction or degradation of the extracellular scaffold and destroy all traces of the vascular and nerves. Once the scaffold is prepared, human cells are seeded so they can proliferate, migrate, and differentiate into the specific tissue. The intent of most

decellularization processes is to minimize the disruption to the underlying scaffold and thus retain native mechanical properties and biologic properties of the tissue but, to date, this has not been achieved.

Of fundamental importance to the survival of most engineered tissues is gas and nutrient exchange. In nature, this is accomplished by virtue of microcirculation, which is the feeding of oxygen and nutrients to tissues and removing waste at the capillary level. However, gas exchange in most engineered tissues is typically accomplished passively by diffusion (generally over distances less than 1 mm), or actively by elution of oxygen from specific types of material fibers[45]. Microcirculation is difficult to engineer, particularly because the cross-sectional dimension of a capillary is on the order of 5 to 10 micrometers (μm; microns) in diameter. As yet, the manufacturing processes for engineering tissue scaffolds have not been developed and are not capable of creating a network of blood vessels. Currently, there are no known tissue engineering scaffolds with a circulation designed into the structure for gas exchange. As a result, the scaffolds for tissues and organs are limited in size and shape.

Introduction to Biofabrication

Natural polymers such as silk, collagen and chitosan are attractive as biomaterials with possible applications for implants, scaffolds in tissue engineering, and biomedical devices. The use of natural and synthetic polymers as scaffolding materials for tissue engineering and regenerative medicine is far from clinical applications primarily due to the lack of manufacturing control over the three-dimensional architecture, a crucial factor influencing cell migration, attachment, differentiation and the production of extracellular matrix[46]. Viable solutions for implants, as well as scaffolds for tissue engineering, require fabrication methods in which the assembly of biomaterials can be controlled on the nanoscale to "remind" cells of the nanotopography of their natural extracellular matrix[47].

Traditional manufacturing methods for small-scale devices, such as microfabrication, have limitations with regard to control of shape and size. Since top-down manufacturing methods are inadequate for manufacturing larger complex nano-sized devices, there is an emerging interest in using biological systems for manufacturing. Biofabrication, the combination of biology and microfabrication, may be the future solution for the production of complex 3D architecture with nanoscale precision [2]. A spider weaving a web is an example of a biofabrication process. Biofabrication can be used to assemble layers of nano-sized fibrils with precision. Biological assembly can be affected by various stimuli such as electrical fields, magnetic fields, temperature, pH, or chemical gradients. Biofabrication of natural polymers, such as spider silk and cellulose, has great potential to overcome the limitations of scaffold production for regenerative medicine.

Chapter 3 : Morphological Control

4.1 Methods

a. Bacteria Cellulose Synthesis

The strain *Acetobacter xylinum* subsp.sucrofermentas BPR2001, (700178, American Type Culture Collection) was used for all experiments. Modified fructose media with an addition of corn steep liquid (CSL) [28, 48], with a conductivity of approximately 7.5 mS/cm and a pH of 5.5, was used as the culture media. Six cellulose-forming colonies were cultured for 2 days at 30ºC in a rough flask (nominal volume, 300ml; working volume, 100ml) yielding a cell concentration of $3.7*10^6$ cfu/ml. The bacteria were then liberated by vigorous shaking and inoculated into new culture media.

The velocity of the bacterial cells under the influence of an electric field and the electrokinetic mobility were evaluated in a microfluidic channel. The effect of an electric field on cellulose production was then evaluated in micro-growth chambers. The small dimension of these chambers minimized the contribution of gravity and buoyancy and isolated the bacteria from atmospheric oxygen. Cellulose production under an electric field was then evaluated in 15mL test tubes, 100mL beaker, and cell culture chambers.

b. Microfluidic Device Fabrication

A silicon master stamp was fabricated on a <100> silicon substrate. AZ 9260 (AZ Electronic Materials) photoresist was spun onto a clean silicon wafer and soft baked at 114C for 45 seconds (Figure 5a). The wafer was then exposed to UV light for 45 seconds with an intensity of 12 W/m through a chrome plated glass mask. The exposed photoresist was then removed using Potassium based buffered developer AZ400K followed by another hard baking at 115C for 45 seconds (Figure 5b). Deep Reactive Ion Etching (DRIE) was used to etch the silicon master stamp to depths ranging from 50-100 microns (Figure 5c). The silicon master stamp was then cleaned with acetone to remove any remaining photoresist (Figure 5d). The scalloping effect, a typical effect of the DRIE etching method, creates a surface roughness which is detrimental to the stamping process. In order to reduce the surface roughness, silicon oxide was grown on the silicon master using thermal oxidation and then was removed as shown in Figure 6.

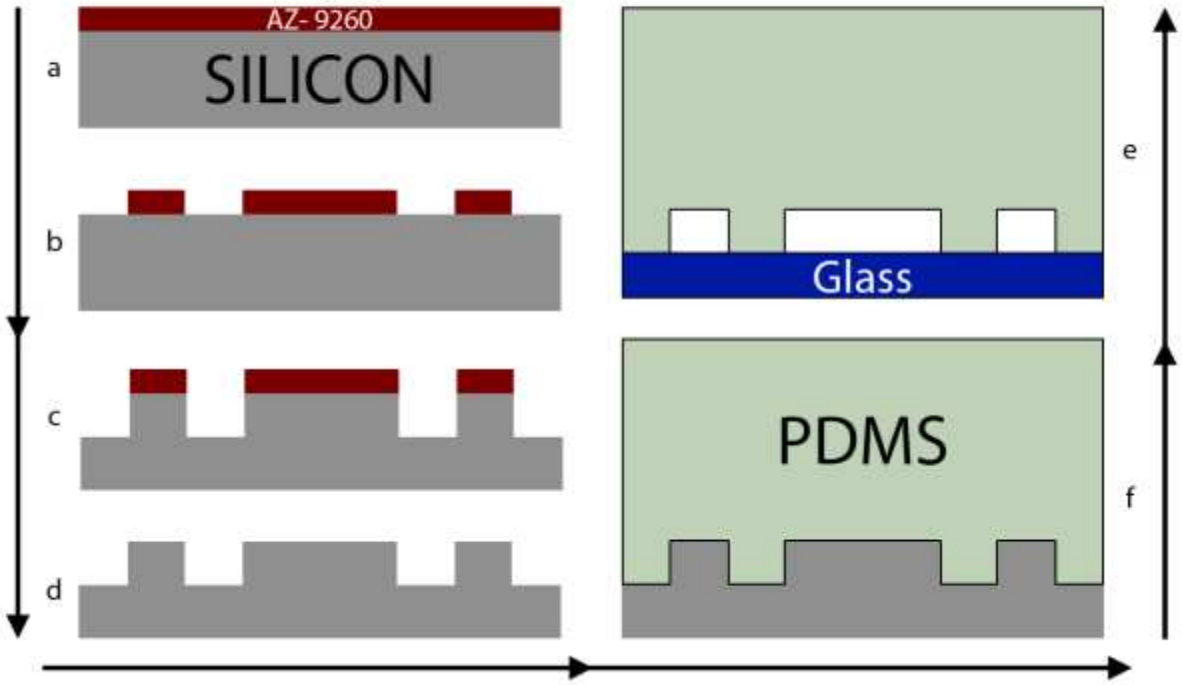

Figure 5: (a) Schematic of the fabrication process used to create the microfluidic chambers. Steps a through d are followed only once to create a master stamp. Steps e and f are repeated to produce an indefinite number of experimental devices.

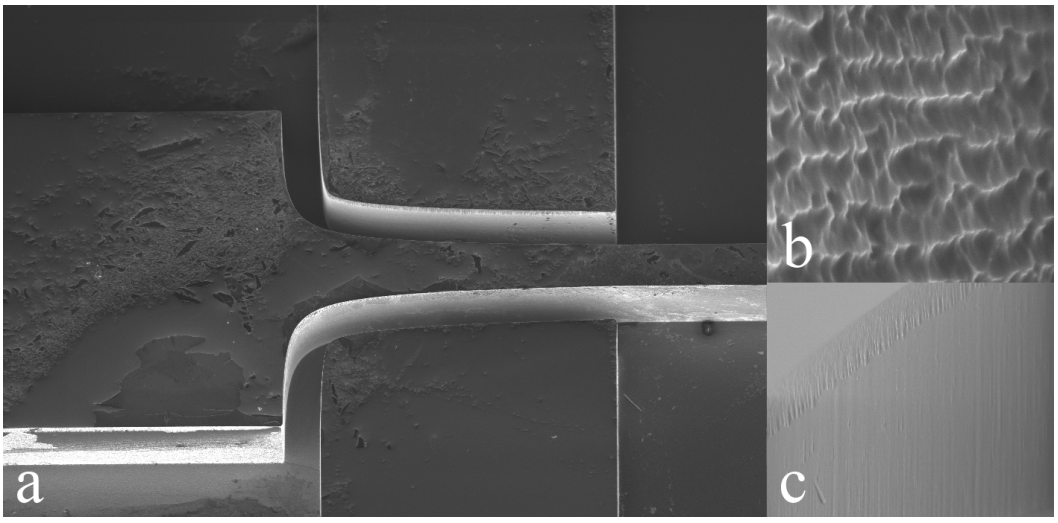

Figure 6: (a) SEM image of the silicon wafer mold at the intersection between the side and the main channel of the microfluidic device (b) Scalloping effect after DRIE (c) surface roughness of the wafer after growing and removing the oxide layer.

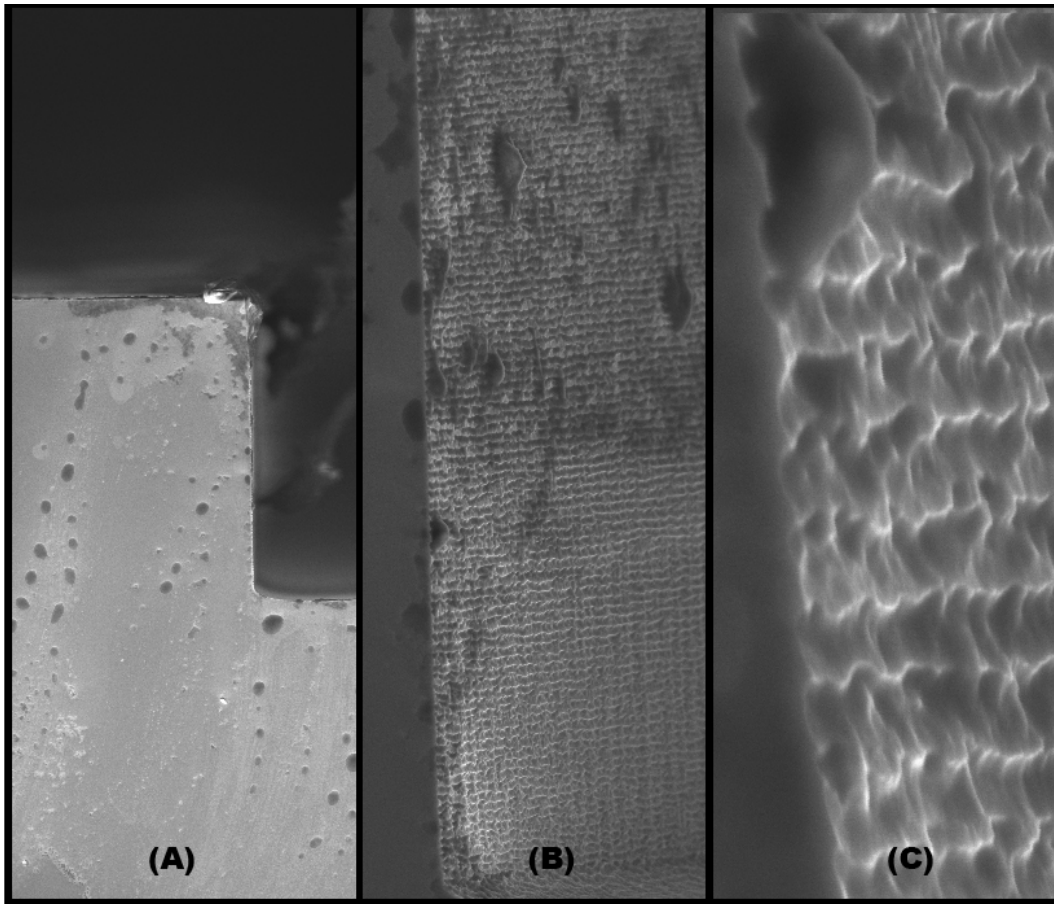

Figure 7: Magnified visualization of the DRIE scalloping effect.

The liquid phase PDMS was made by mixing the PDMS monomers and the curing agent in a 10:1 ratio (Sylgrad 184, Dow Corning, USA). The bubbles in the liquid PDMS were removed by exposing the mixture to vacuum for an hour. An enclosure was created around the wafer using aluminum foil in order to contain the PDMS on the wafer as well as to ensure the proper depth for the PDMS portion of the device. The clean PDMS liquid was then poured onto the silicon master and 15 minutes was allowed for degassing. The PDMS was then cured for 10 min at 150°C and then removed from the mold. Finally, fluidic connections to the channels were punched with 15 gauge blunt needles (Howard Electronic Instruments, USA).

A glass microscope slide (3" X 2" X 1.2mm, Fisher Scientific, USA) and the PDMS replica were cleaned with soap and water and rinsed with ethanol, and distilled water then dried with a compressed air. The PDMS and glass were exposed to air plasma for two minutes on high in a PDC-001 plasma cleaner (Harrick Plasma, Ithaca, NY). After exposure, the layers were immediately brought into contact and pressure was applied by rolling a plastic tube on top of the PDMS layer.

Blunt dispensing needles (JG18-1.0P, Howard Electronic Instruments Inc, El Dorado, KS) were used to provide fluid and electrical connections to the microfluidic channels. Luer-slip plastic syringes were used as large fluid reservoirs (3ml S7510-3, National Scientific Company, Rockwood, TN). A programmable DC power supply (PSP-405, GW Instek America Corp, Chino, CA) was used to induce an electric field within the channels. An inverted light microscope (Leica DMI 6000B, Leica Microsystems, Bannockburn, IL) equipped with a digital camera (Hamamatsu EM-CCD C9100, Hamamatsu Photonics K.K. Shizuoka Pref., 430-8587, Japan) was used to monitor the velocity of cells in the channel.

Bacterial cells inoculated in media were fluorescently stained with BacLight™ (Invitrogen, Carlsbad, CA) and injected into a 1cm long 300 micron wide 50 micron deep straight microfluidic channel. The reservoirs were filled and pressure was allowed to equalize prior to the application of electric fields. Cell velocities were measured by acquiring high speed video and measuring pixel translation over 15 seconds.

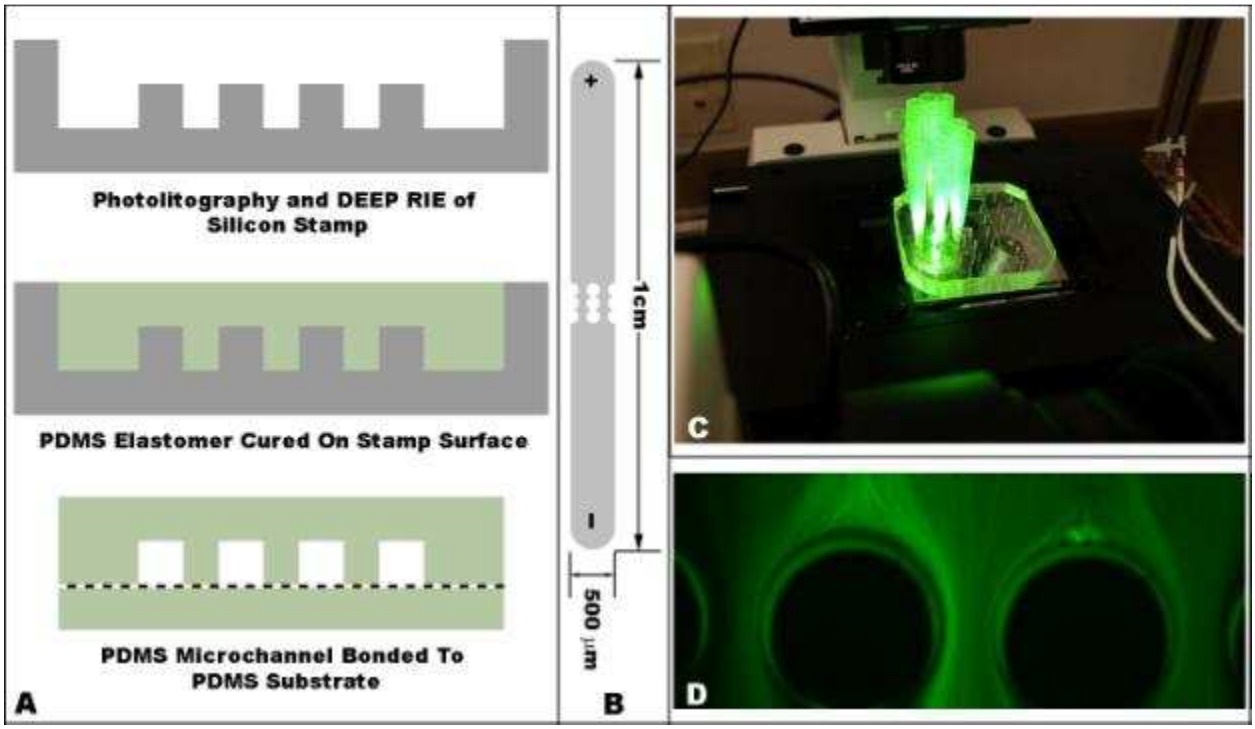

Figure 8: a) Fabrication process for creating microfluidic channels. b) Schematic showing the top view of the channels with insulating pillars. c) Experimental setup for interfacing with microfluidic channels. 1000uL pipette tips are used as fluid reservoirs to maintain pressure equilibrium across the channel. d) Time lapse images of fluorescently labeled A. xylinum cells being controlled through the microfluidic channel by electrokinetic and dielectrophoretic forces.

c. Microfluidic Device Cellulose Synthesis

A. xylinum cells were then inoculated into culture media and injected into the microfluidic channels. Fluid flow was halted by adding 100mL of additional culture media to each inlet reservoir and pressure difference was allowed to equalize. Platinum electrodes were used to apply small electric fields across the channels inducing electrokinetic and dielectrophoretic forces that guided the bacterial cells as they produced cellulose nanofibers. After 48 hours, cellulose production was halted by quenching the scaffolds in liquid nitrogen.

d. Fabrication of Micro-Growth Chambers for Cellulose Network Synthesis

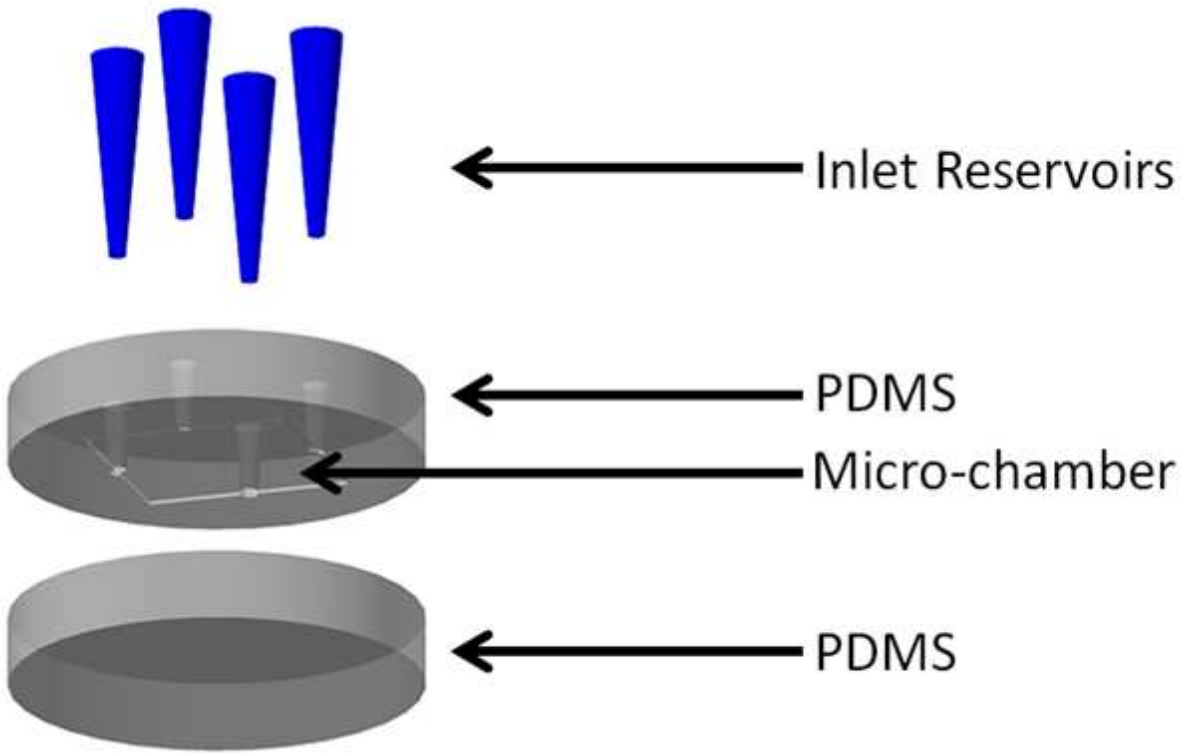

Figure 9: Schematic of the experimental PDMS micro-chamber.

Micro-growth chamber stamps were fabricated by cleaving unaltered 500 micron thick silicon wafers into rectangles measuring 4.5x0.5cm. These rectangles were then adhered to a glass slide as shown in Figure 10. A liquid phase elastomer was made by mixing PDMS monomers and the curing agent in the ratio of 10:1 (Sylgrad 184, Dow Corning, USA). The bubbles in the liquid PDMS were removed by exposing the mixture to vacuum for an hour. The PDMS liquid was then poured onto the silicon master that was encased by aluminum foil, producing a thickness of 1cm. Any remaining bubbles were allotted 15 minutes to float to the surface. The PDMS was then cured for 10 minutes at 150oC and peeled off the stamp. Inlet ports to each channel were punched using sharpened dispensing needles (JG14-1.0P, Jensen Global Inc, Santa Barbara, CA).

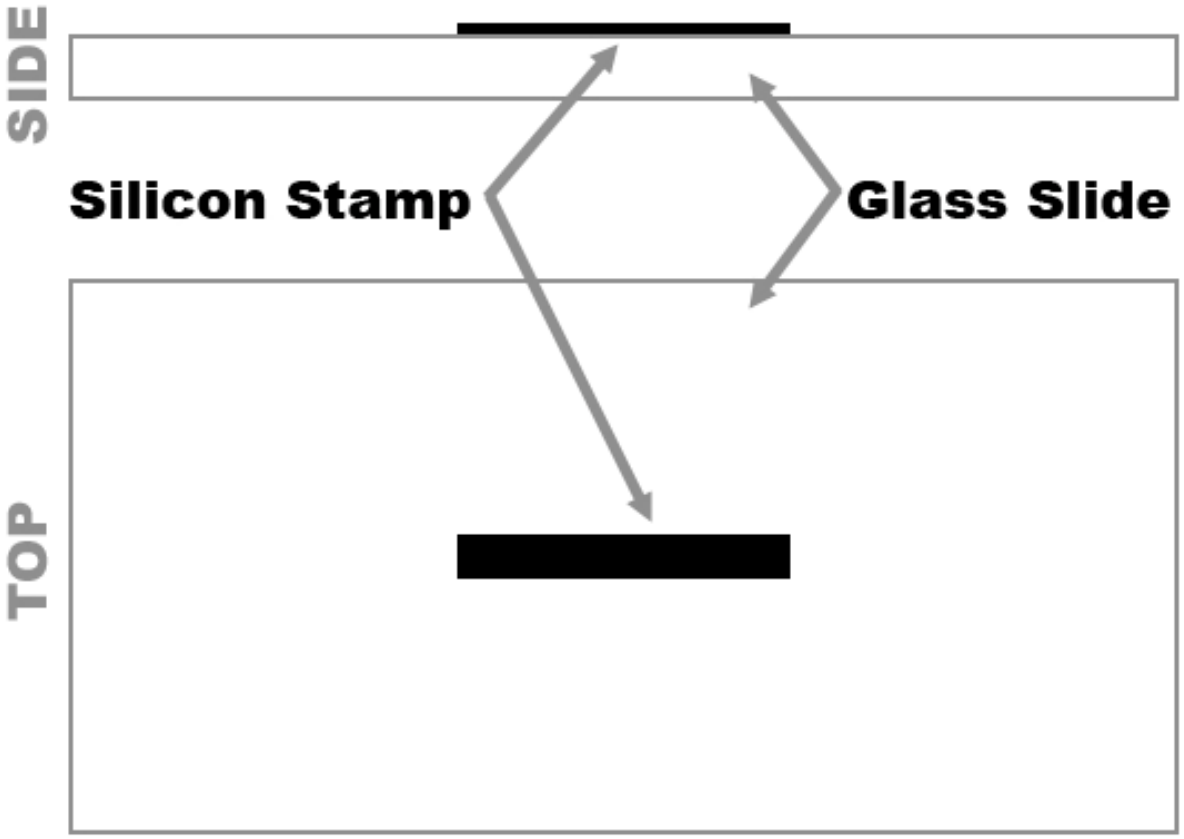

Figure 10: Schematic of the silicon on glass stamp used to create micro-growth chambers.

The PDMS device layer of the micro-growth chamber and a flat piece of PDMS were washed using soap and water then rinsed in ethanol, isopropanol, and deionized water, then dried using pressurized air. Both were then exposed to air plasma for 2 minutes on high in a PDC-001 plasma cleaner (Harrick Plasma, Ithaca, NY). After exposure, the layers were immediately brought into contact and pressure was applied by rolling a plastic tube on top of the PDMS layer. This yielded a semi-permanent, water tight bond and the devices could be separated by gently pulling the two layers apart allowing samples to be removed after culture. The chambers remained under pressure a minimum of 10 minutes and were stored in a vacuum chamber until use.

Figure 11: Silicon stamps covered in PDMS during the stamping process. Foil is used to create a mould, distribute heat, and prevent PDMS from leaking.

e. *Micro–Growth Chamber Cellulose Production*

The micro-growth chamber was first cleaned with ethanol and rinsed with deionized water before priming with 100µL of inoculated culture media. Two 1000µL pipette tips were inserted into the inlets of the micro-environment and used as media reservoirs. Aluminium electrodes (22Gage 99.99%, Electron Microscopy Sciences, Hatfield, PA) were then placed in the reservoirs and electric fields between 0.1 (0.45V) and 5V/cm (22.5V) were applied using a DC power supply (Model 72-7245, Tenma Electronics, Delaware). Cultivation was allowed to proceed for 72 hours before the electric field was removed. The micro-environments were then opened and the resulting cellulose networks were placed in liquid nitrogen to halt cellulose production.

The materials were then freeze dried in a Labonco FreeZone 2.5 Plus (Labconco Corp., Kansas City, Missouri) freeze dryer for 48 hours without any further processing to leave the bacterial cells in situ. 5nm of gold was then deposited on the scaffold and Field Emission Scanning Electron Microscopy (FESEM) was conducted at a working distance of 6mm and 5kV electron beam intensity using a LEO Zeiss 1550 FESEM (Carl Zeiss SMT, Oberkochen, Germany).

f. 15 mL Test Tube Cellulose Production

Two small holes were drilled into the lid of 15mL test tubes. The caps and tubes were rinsed with soap and water, ethanol, then DI water. They were then filled with 11mL of inoculated culture media. Aluminum electrodes were inserted into the test tubes through the holes in the cap. 1V, 2.5V, and 5V DC (approximately 0.67V/cm, 1.67V/cm, and 3.33V/cm electric field) signals were applied across the electrodes for 24 hours while the cultivation of the bacteria persisted. The contents of the test tubes were emptied into individual aluminium foil dishes and dried overnight at 95°C to recover the dry weight of cellulose produced. The electric current passing through the test tube was measured using a digital multimeter (197 Autoranging Microvolt DMM, Keithley Instruments, Cleveland, Ohio). From these values, the volume of oxygen released via electrolysis can was estimated using Faraday's law of electrolysis

$$m = \left(\frac{Q}{F}\right)\left(\frac{M}{z}\right) \tag{42.}$$

$$Q = I \cdot t \tag{43.}$$

where Q is the total charge delivered, I is the average current, t is the time, F is Faraday's constant, M is the molar mass of oxygen, and z is the valence number. The number of moles produced is calculated by dividing the mass (m) by the molar mass (M)

$$n = \left(\frac{I \cdot t}{F}\right)\left(\frac{1}{z}\right) \tag{44.}$$

From this, the total volume of oxygen produced (V) can be calculated through the ideal gas law

$$P \cdot V = n \cdot R \cdot T \tag{45.}$$

where P is atmospheric pressure, R is the ideal gas constant, and T is ambient temperature.

g. 100 mL Beaker Cellulose Production

A 100mL beaker was filled with 10mL of inoculated culture media. Then aluminium electrodes were inserted along opposing edges of the beaker. Fields of 1.1V/cm to 4.4V/cm (5V DC through 20V DC) were applied across the electrodes and cultivation was allowed to persist for 20 minutes. The fibres produced were immediately stained with Calcoflour White (Becton, Dikenson and Company, Sparks, MD) and imaged using fluorescent microscopy (Leica DMI 6000B and A4 Filter cube, Leica Microsystems, Bannockburn, IL).

h. 10mL OptiCell 1100 Cellulose Production

OptiCell 1100 cell culture chambers (Thermo Fisher Scientific, Waltham, MA) were filled with 10mL of inoculated culture media. Then aluminum electrodes were then carefully inserted into the chambers via

the syringe inlets. Fields of 0.077V/cm to 0.77V/cm (0.5V to 5.0V DC) were applied across the electrodes and cultivation was allowed to persist for 5 days. The electric field was then removed and the culture chambers were heated in a water bath at 60°C for a minimum of 1 hour to halt cellulose production.

4.2 Results

a. Microfluidic Device Results

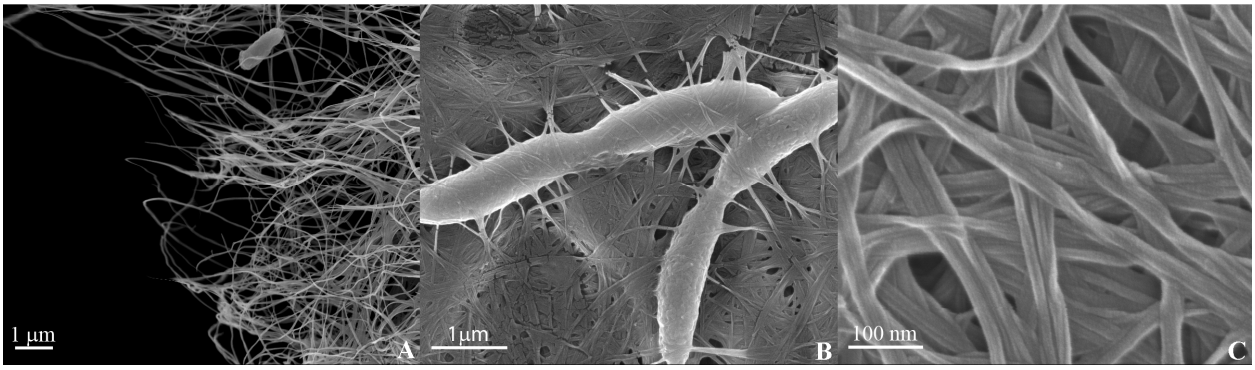

Figure 12: (a) A single A. xylinum cell is entangled in the dense random cellulose network it helped produce. (b) Two A. xylinum cells embedded in a cellulose network undergoing mitosis. (c) The random nanocellulose network produced by A. *xylinum.*

Acetobacter xylinum can be controlled electrically. When placed in a hemocytometer 100 microns deep and a voltage of 10V applied the bacteria move in the direction of the applied electric field with a velocity of 400microns/minute. When compared to control samples as in Figure 14, the net movement under an electric field is in the direction of the applied field. The path of the bacterium is not perfectly linear due to movement of the bacteria due to metabolic processes, Brownian motion, and cellulose production.

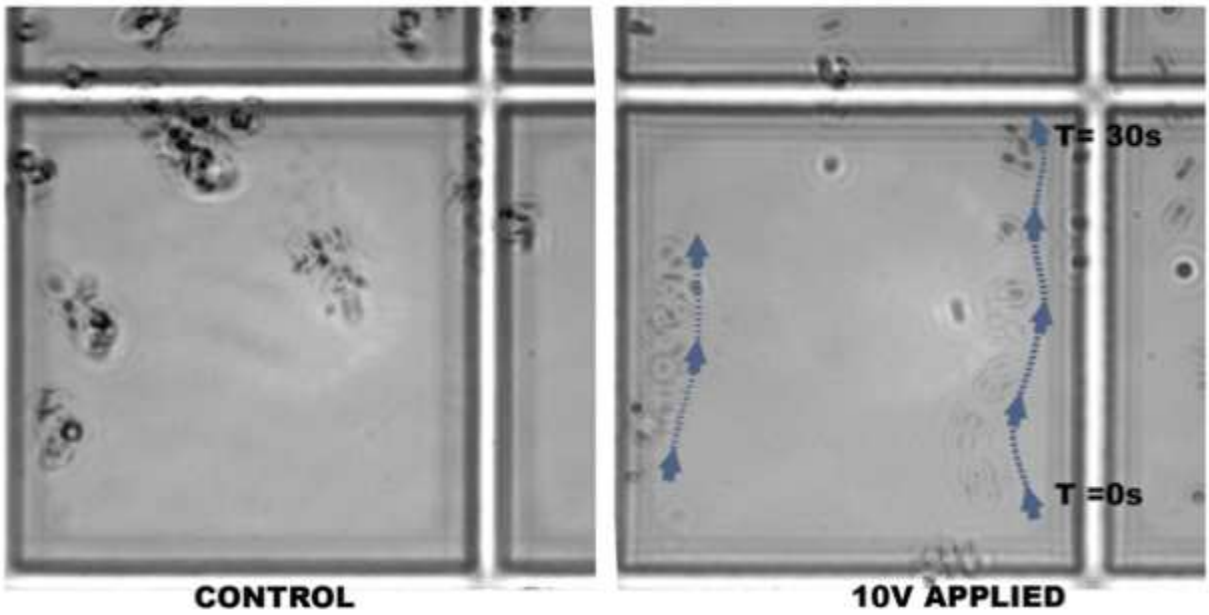

Figure 14: Time lapse image of controlled electrokinetic movement of *Acetobacter xylinum* a distance of 200µm over 30 seconds with a 10V applied electric field. Control experiments have no net movement.

In the microfluidic channels, the velocity of the bacterium while the electric field was turned off was measured to be 0.44µm/min ± .123µm/min. This velocity was due to very small pressure differences between the inlet and outlet reservoirs. The average velocity of the bacterial cells increased from 1.37µm/min to 7.47µm/min as the electric field was increased from 2V/cm to 30V/cm as seen in Figure 13. Based on these experiments the average electrokinetic mobility was calculated to be —. The electrokinetic velocity of the bacteria at electric field strengths lower than 2.0 V/cm was too close to the pressure-induced velocity to be measured accurately in the experimental setup, but has been theoretically estimated based on electrokinetic mobility as seen in the semi-log plot in Figure 13(bottom).

The progression of bacteria labeled with BacLight™ (Invitrogen, Carlsbad, CA) through the channel is

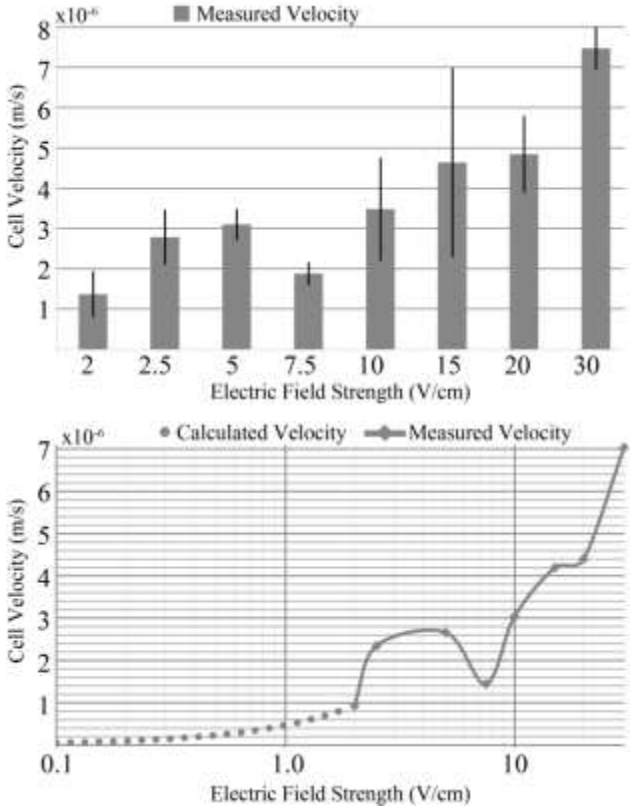

Figure 13: The electrokinetic velocity of bacterial cells (top) measured for electric field strengths between 2V/cm and 30V/cm and (bottom) calculated velocity based on electrokinetic mobility.

shown in Figure 15 and Figure 16. Under an applied field, the bacteria are electrokinetically driven through the channel. Insulating pillars and variations in the geometry of the channel induce dielectrophoretic forces which can also be used to direct the bacteria.

The dielectrophoretic forces become more dominant in directing the bacteria as $\vec{E}$ is increased and above 400V/cm the bacteria are held in place and concentrated near the insulating pillars (Figure 17). It should be noted that at this field strength, the bacteria switch off cellulose production. These results show that even though the parameters μ_{ek} and μ_{DEP} are intrinsic properties of the bacteria in their culture media, $\vec{E}$ can be varied to control bacteria motion.

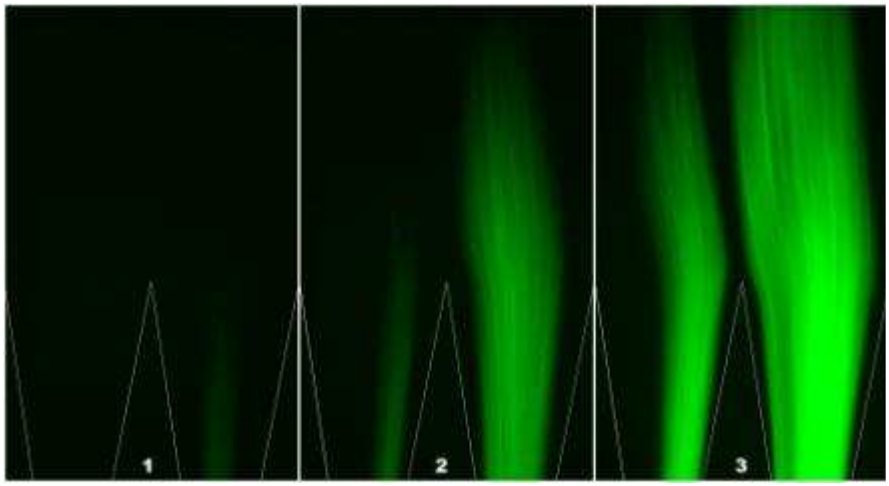

Figure 15: Time lapse images of fluorescently labeled A. xylinum cells being moved through a microfluidic chamber by electrokinetic and dielectrophoretic forces.

Due to the small scale of these devices and the strength of the PDMS-Glass bond, removal of cellulose produced in these channels was difficult and sample sizes were too small for mechanical evaluation. The results from these experiments where however, useful in determining relevant parameters for future experiments.

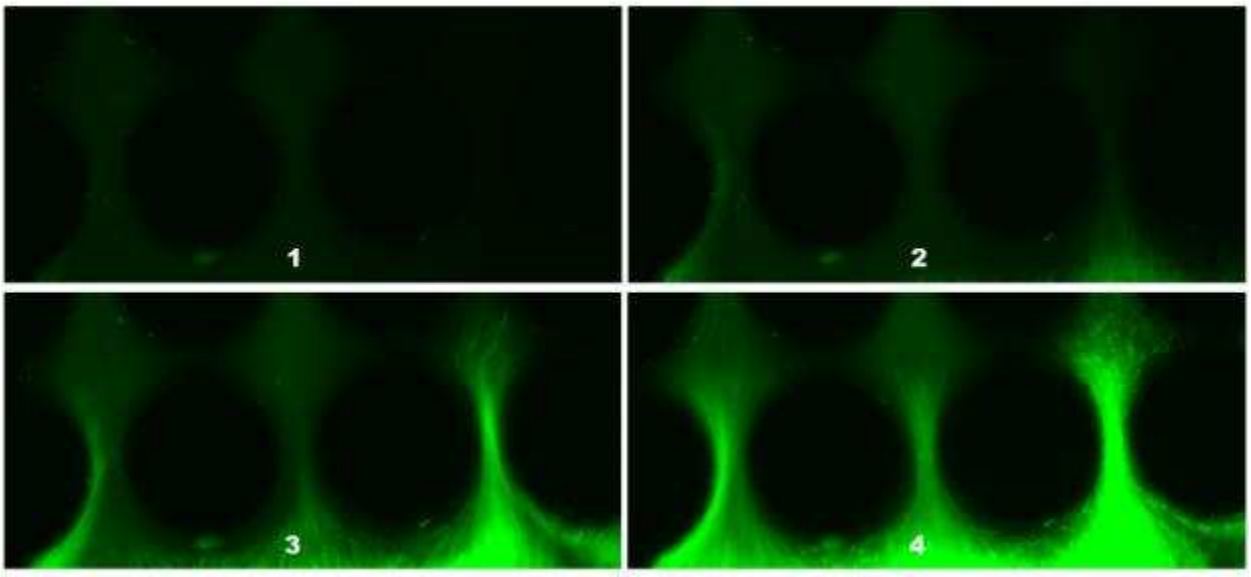

Figure 16 Additional time lapse images of fluorescently labeled A. xylinum cells being moved through a microfluidic chamber by electrokinetic and dielectrophoretic forces

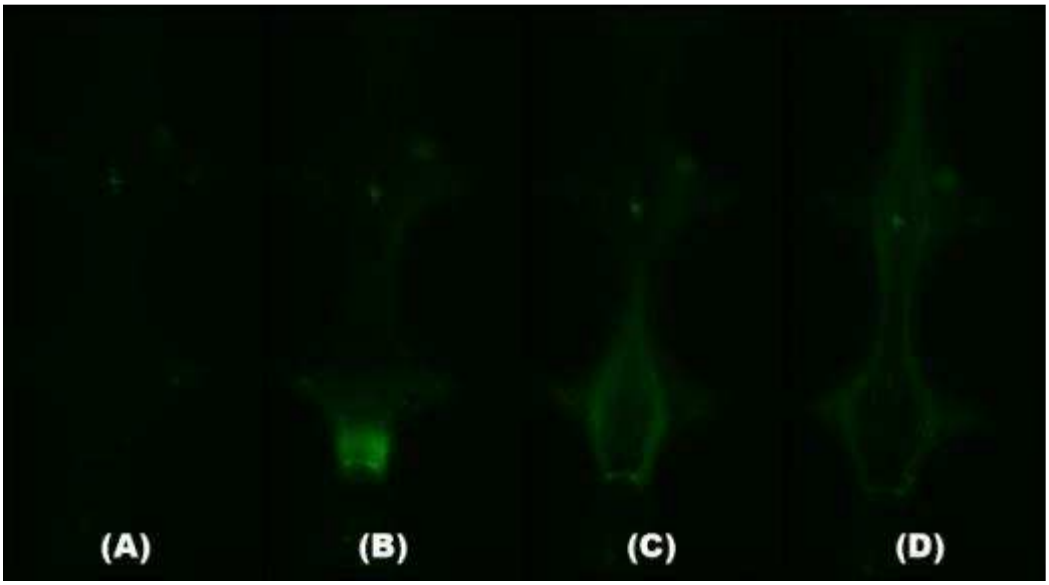

Figure 17: Acetobacter xylinum (A) driven through a micrifluidic channel by electrokinetic foces, (B) trapped by dielectrophoretic forces under the application of 400V/cm , and (C-D) selectivly released by

b. Micro-Growth Chamber Results

The micro-growth chambers provided the optimum platform for producing cellulose scaffolds for visualization. Without an applied electric field, the bacteria produce a dense random network as seen in Figure 18a, and as reported previously by numerous authors [29-32, 49-51]. Under high electrical fields, cellulose production is switched off. However, there are experimental conditions in which the motion of the bacteria can be controlled while simultaneously producing cellulose. Cellulose networks produced under 0.15V/cm, 0.303V/cm and 0.45V/cm are different in structure than those produced in static culture and are visible in Figure 18.

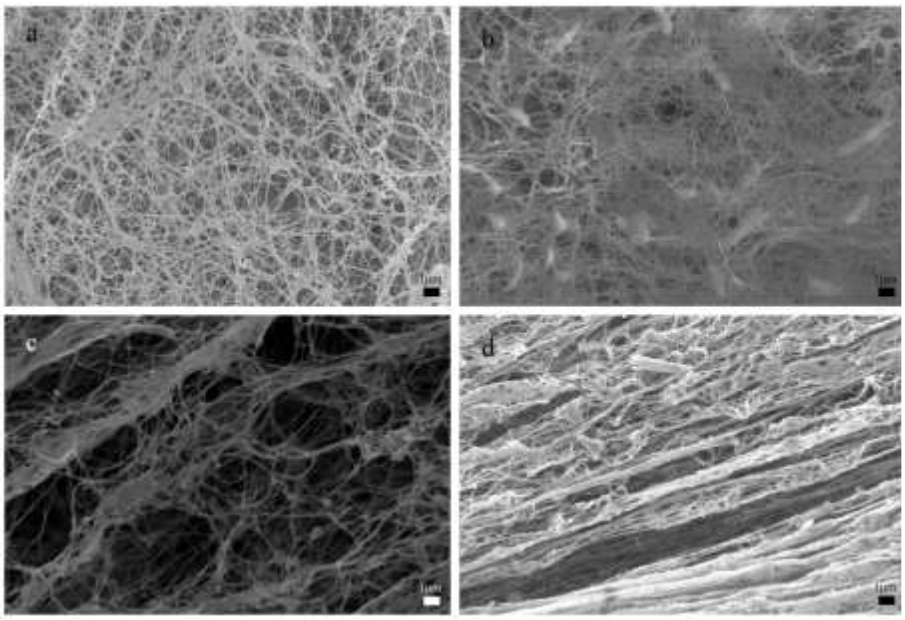

Figure 18: SEM images of the cellulose networks produced under a) 0V/cm, b)0.15V/cm, c)0.303V/cm, d)0.45V/cm at 5000x magnification

Under these experimental conditions, the bacterial cells were experiencing a calculated electrokinetic velocity between 4.2µm/min and 12.6µm/min. During the cultivation process, bacteria are likely traveling at slower velocities due to the action of fluid drag forces and tensile forces from interacting cellulose fibers which were not quantified.

Under static culture conditions, *A. xylinum* extrude cellulose at an average rate of 2µm/min[21]. We hypothesize that electrokinetic forces due to electric fields between 0.1V/cm and 1V/cm are moving at average velocities in proximity to this production rate. At electrokinetic velocities below 2µm/min, the cellulose network produced is not greatly affected. The bacteria observed via light microscopy tended to tumble and move randomly in static culture and this behavior reflected similarly at low electric field strengths. The slightly less dense network observed under 0.15V/cm (2b) is similar to those described by others under slow shaking of the culture broth [52]. At this electric field strength, the bacteria are being moved enough to affect the density of the network, but not produce any overall change in fiber alignment. As the electric field intensity is increased, the electrokinetic movement of the bacteria begins to influence the organization of the cellulose network produced.

The cellulose network in Figure 19 was created under the influence of a 0.303V/cm electric field. At this field strength, groups of fibers can be seen aligned in one direction at 500x magnification (Figure 19a). Examination of the network at 2000x and 5000x magnification (Figure 19b and c respectively) reveals a branching network intersecting the aligned fibers. The induced velocity of the bacteria may be very close

to the natural extrusion rate, having an influence on overall translational movement, but not strong enough to drive fiber extrusion exclusively in one direction.

Figure 20 demonstrates a stranded cellulose network produced under 0.45V/cm. At this electric field strength, the movement of the bacteria is strong enough to limit the formation of cellulose strands perpendicular to the applied field. Examination of this network under 40000x magnification shows numerous fibers from individual bacterium having been pulled together to form larger structures.

As electric field strengths in the micro-growth chambers increase, the formation of solid cellulose structures ceases. The velocity of the cells in this case may be too high resulting in either diminished cellulose production (similar to vigorous agitation), the electric field interfering with cellular function[20, 53-56], or the expression of non-cellulose producing phenotypes[57]. Evaluation of these mechanisms and the material produced will be the subject of future work.

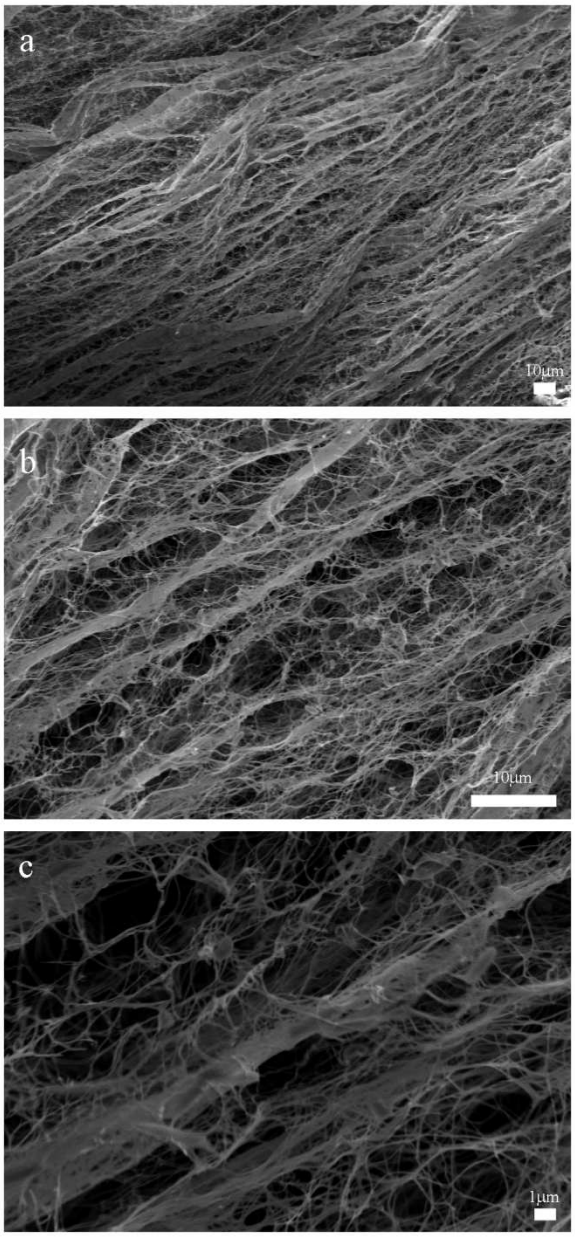

Figure 19: Cellulose network produced under a 0.303V/cm electric field at (a) 500x (a), (b) 2000x (b) and (c) 5000x (c) magnification.

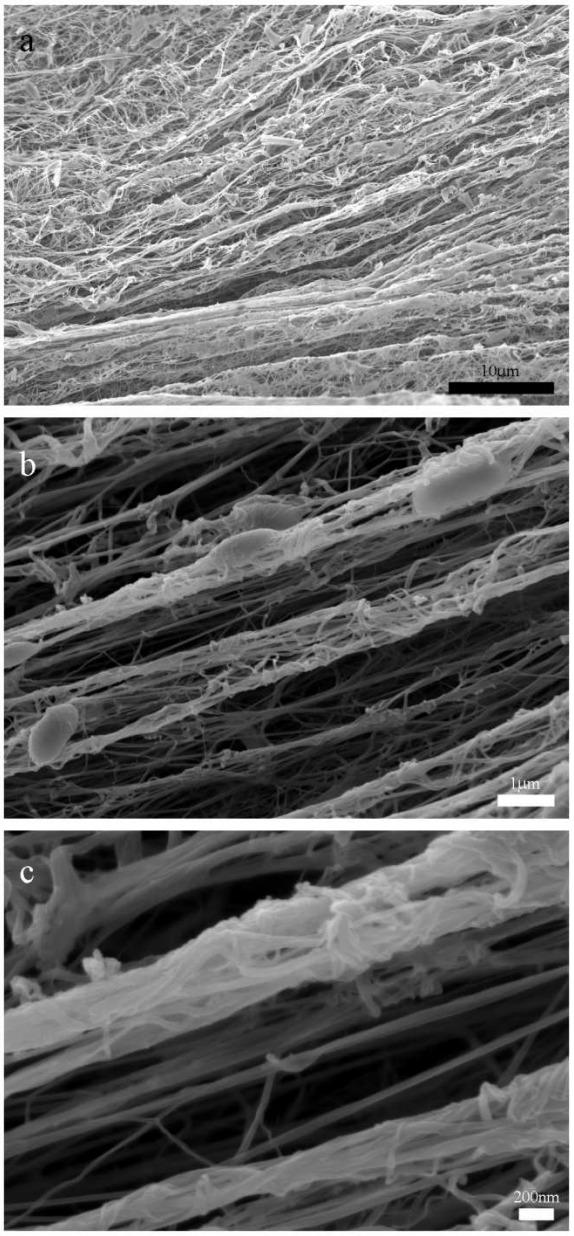

Figure 20: Cellulose network produced under a 0.45V/cm electric field at (a) 2500x, (b) 1344x and (c) 4000x magnification

c. 15mL Test Tube Results

Cellulose production by *Acetobacter xylinum* typically only occurs at the liquid-air boundary. In control cases, a single thin layer of cellulose is produced. Production of multiple layers of specified thickness is achievable by adding small quantities of culture media on top of an existing layer. As the new media coats the existing layer, bacteria in that layer begin to rise to the new nutrient rich liquid-air boundary as seen in Figure 21. The thickness of each layer can be controlled by adjusting the rate at which new media is added on top of the highest layer. Thickness is however, limited to the native formation thickness which is limited by the ability of the bacteria to receive oxygen from the air.

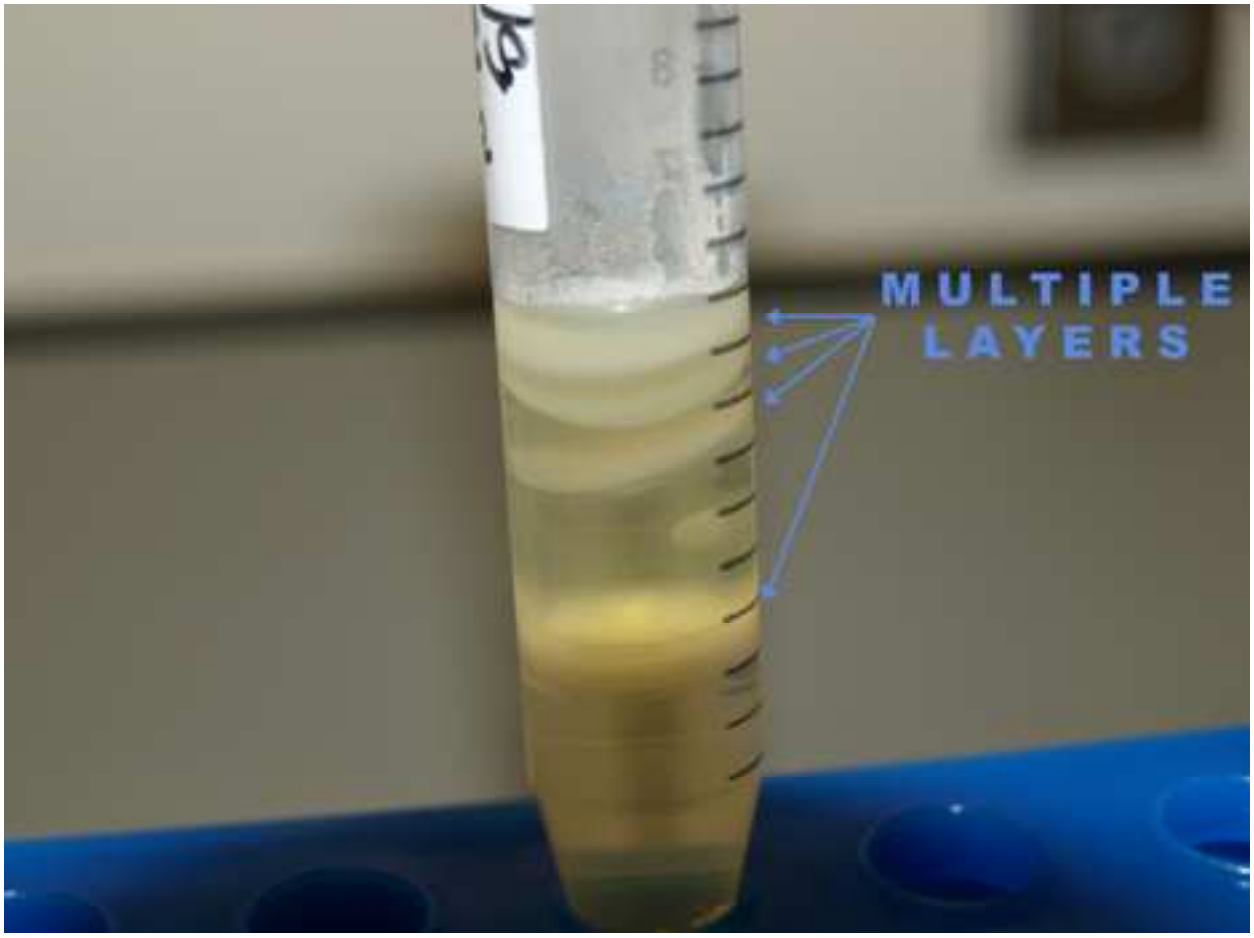

Figure 21: Cellulose growth in multiple layers by adding small quantities of culture media at discrete time points

Cellulose production in a test tube is altered dramatically under the presence of an electric field. In static culture with no electric field, cellulose production occurs only at the liquid-air boundary. For voltages less than 1V, significant cellulose production below the liquid-air boundary was not observed. For voltages greater than 1V (0.67V/cm) cellulose production is induced and this resulted in significant cellulose production below the liquid-air boundary. At 1V, cellulose production increased by 2.9 percent. While this value is not significant, the location of cellulose production shifted from the liquid-air boundary to within the culture media. Under the influence of an electric signals of 2.5V and 5.0V in

magnitude, cellulose production increased by 13.6 and 27.4 percent respectively. This is likely due to the increased production of oxygen via hydrolysis since cellulose production by Acetobacter *xylinum* is primarily an oxygen limited process[58]. At applied voltages above 1V, cellulose production near the oxygen producing anode (positive electrode) is visible. In contrast, the hydrogen producing cathode (negative electrode) had relatively little proximal production throughout the 24 hour period. Experimental current measurements show there is an increase in current through the system between 1.0V and 2.5V, which correlates to an increase in calculated oxygen production and resulted in increased cellulose production. Fiber alignment was not visible under these conditions since 3D effects including gravity and buoyancy influenced the network structure.

d. 100mL Beaker Results

Experiments in 100mL beakers attempted to minimize 3D effects and to limit the influence of macro-scale forces including gravity and buoyancy. Cellulose production was immediately visible at the anode (positive electrode) during the application of 2.2V/cm (10V) and 3.33V/cm (15V) DC. .

As time progressed, a circular region of cellulose around the anode became visible. This circular region began to deform and stretch out towards the cathode as shown in Figure 22 (a). This process is likely due to electrokinetic forces driving the bacterium from one edge of the beaker to the other. The application of 4.44 V/cm (20V) results in minimal cellulose production, and the cells may be moving too fast to produce cellulose chains or their metabolic processes may be impeded in some manner [53-55, 59, 60].

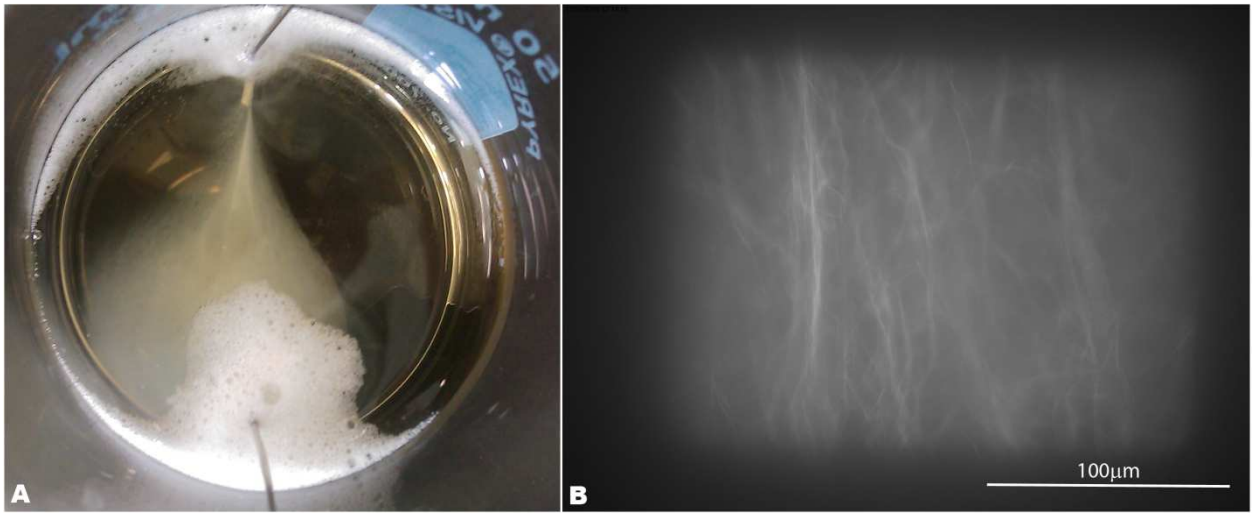

Figure 22: BC Production after 20 minutes in a 100mL beaker w/ 10V applied by aluminum electrodes. (a) Top view. (b) Fibers stained with calcoflour white and imaged with fluorescent microscopy.

e. 10mL Opticell 1100 Results

The OptiCell culture chambers provided an ideal, confined, 2mm thick chamber to observe cellulose production under the application of an electric field. These experiments were conducted with the OptiCell chambers orientated so that the gravitational force was parallel with the electrodes. Without an applied electric field a random cellulose network was produced between the oxygen permeable

membranes. Application of 0.77 V/cm (5V) yielded some cellulose; however, cellulose production was notably diminished. For smaller applied fields, such as 0.31V/cm (2V), cellulose fibers could be seen extending across the chamber after 24 hours. These fibers are not exactly perpendicular to the electrodes due to gravitational forces.

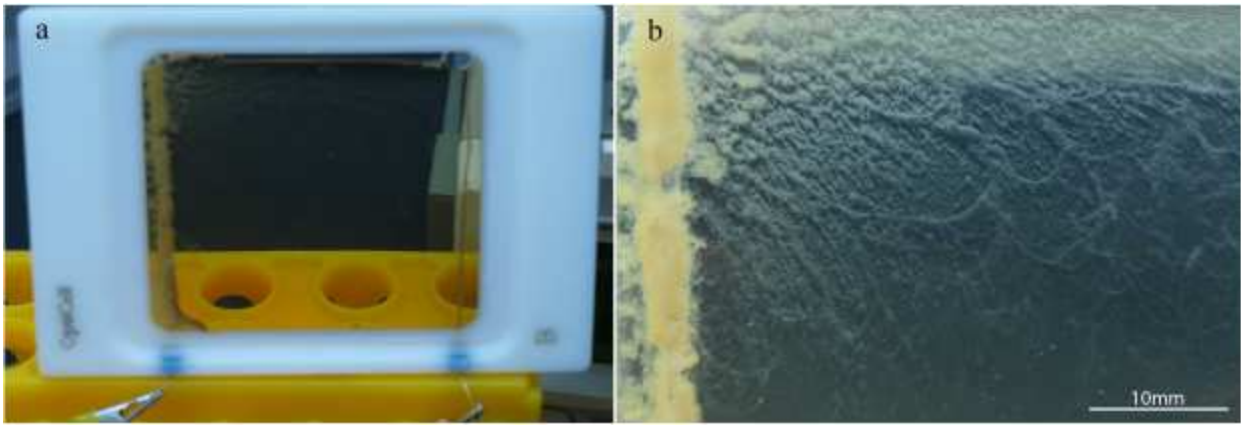

Figure 23 : Fibers stretching across OptiCell culture platform produced by the application of 0.31V/cm (2.0V)

f. Mechanical Testing Results

Stress (σ), is the measure of force per unit area in a deformable body

$$\sigma_{ij} = \frac{F_{ij}}{A} \tag{46.}$$

For a hyperelastic isotropic solid, the linearized constitutive equations are:

$$\begin{aligned} T &= T_{natural} \\ F_{ij} &= I_{ij} \\ T_{ij} &= \lambda E_{ll}\boldsymbol{I} + 2\mu E_{ij} + \alpha_t(T - T_{nat})\boldsymbol{I} \\ q_i &= -k_0 \nabla T \\ E_{ij} &= \frac{1}{2}\left[\nabla u_i + (\nabla u_i)^T\right] \end{aligned} \tag{47.}$$

In the case of simple extension, the stress vector T becomes

$$T_{ij} = \begin{matrix} \sigma & 0 & 0 \\ 0 & 0 & 0 \\ 0 & 0 & 0 \end{matrix} \tag{48.}$$

From this, the stress-strain relationship can easily be determined

$$\begin{aligned} \boldsymbol{\sigma} &= E\boldsymbol{\epsilon} \\ E_{22} &= E_{33} = -\upsilon E_{11} \\ E &= \frac{\mu(3\lambda + 2\mu)}{\lambda + \mu} \end{aligned}$$

$$\upsilon = \frac{1}{2}\frac{\lambda}{\lambda + \mu}$$

where E is Young's modulus and υ is Poisson's ratio.

Preliminary tensile tests were conducted on cellulose networks grown in 4.5x0.5 cm micro-chambers under a number of different conditions including electric fields varying from 0.1 to 2V/cm, with, and without modifications to the culture media.

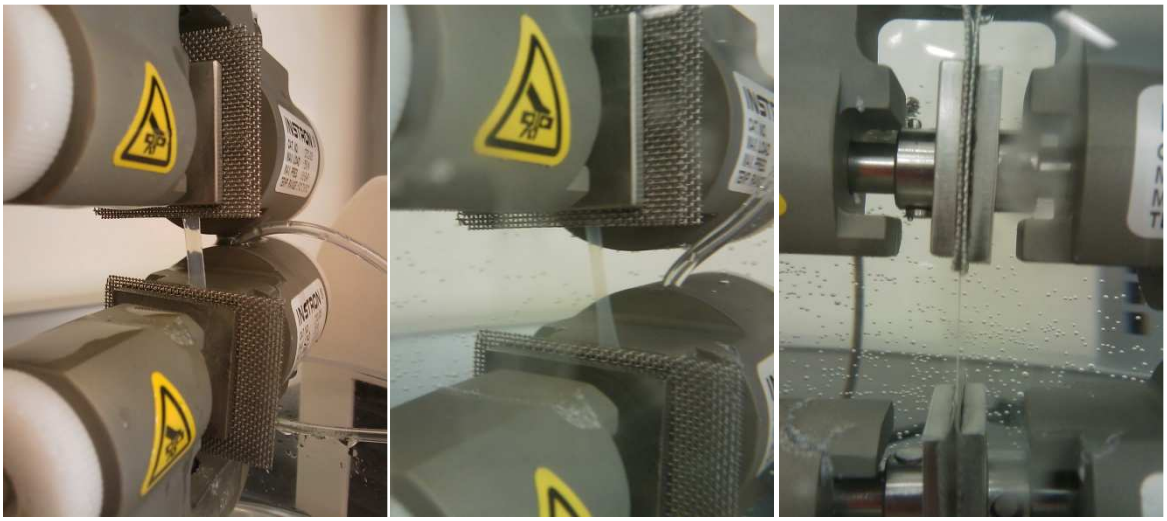

Figure 24: Instron Tensile testing system used to measure the mechanical properties of cellulose networks.

Samples were kept in DI water until just prior to examination. Individual cellulose networks were loaded into the Instron tensile testing setup using metal mesh on either side of each gripper to decrease sample slippage. A water bath filled with DI water at 37C was then raised over the grippers immersing the samples in water. Gage length was then measured and the samples were tested at 10% strain.

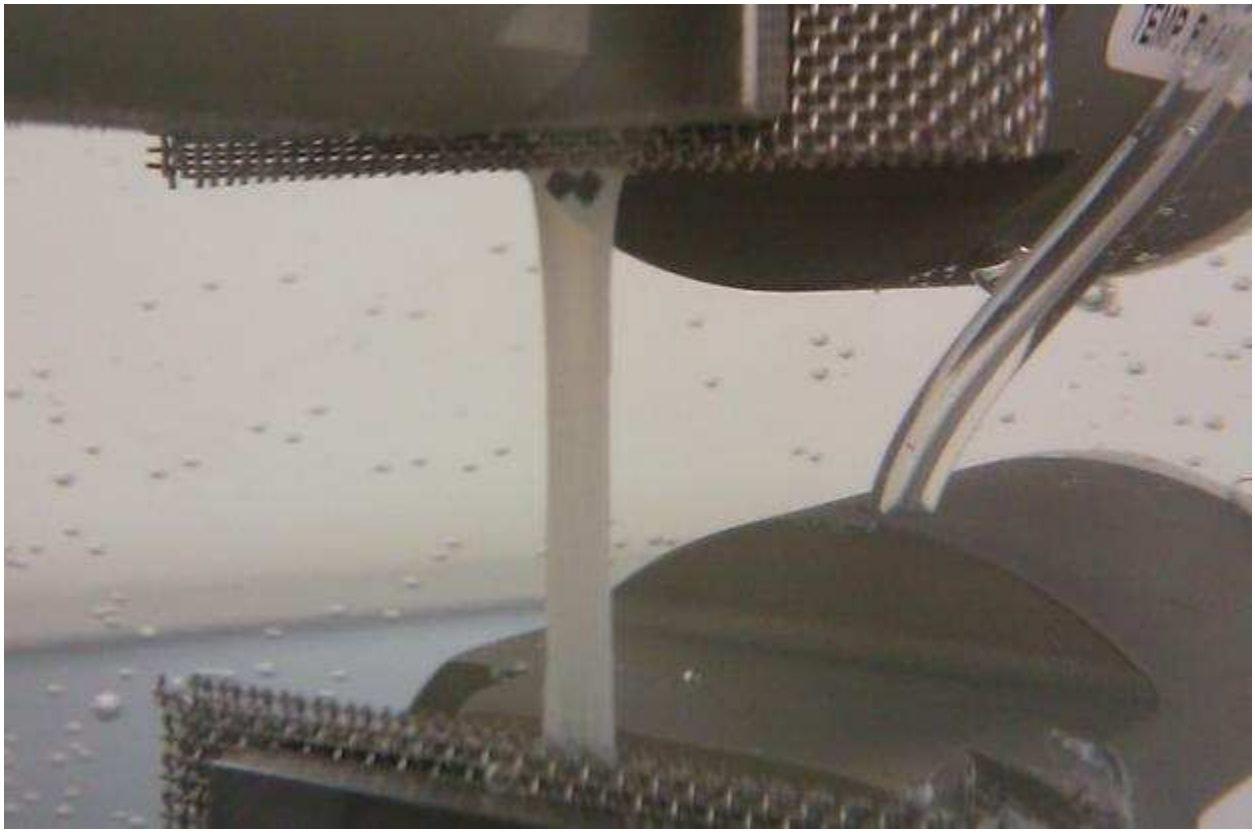

Figure 25: Failure of a cellulose network at the grippers under tensile load.

Tests were allowed to persist until the samples had torn. Samples were not altered once they were removed from the micro-chambers, and a wishbone shape was not cut into the material. This resulted in an atypical failure of the networks, mostly occurring at the intersection of the network and the metal mesh as seen in Figure 25.

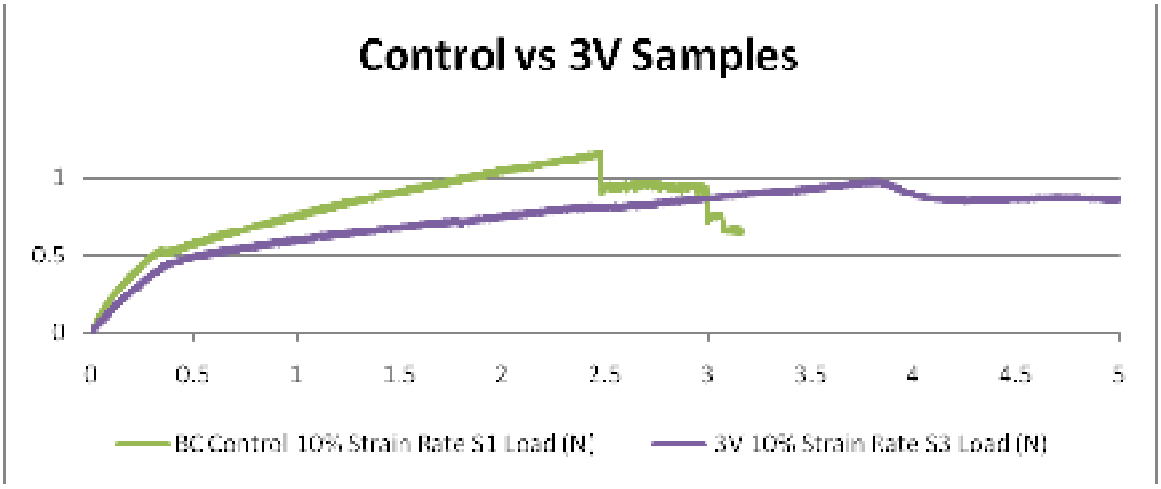

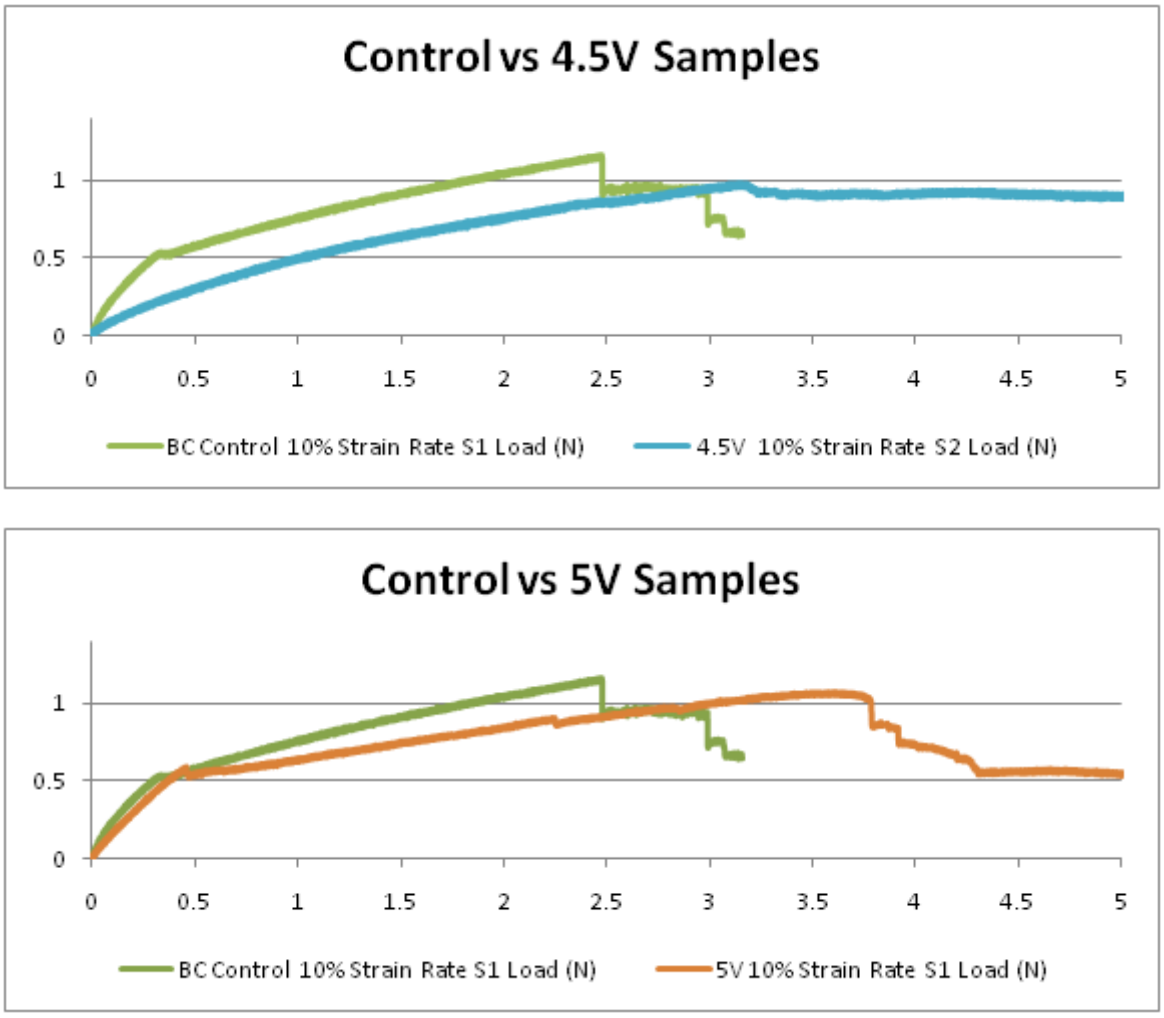

Figure 26: Typical tensile testing results from samples prepared at 2, 4.5, and 5V in a 4.5cm micro-chamber.

Examination of tensile testing data shows that networks grown under an electric field display a longer elongation to break. This suggests that the fibers have become aligned and the network is dissipating energy more efficiently in the axial direction. Nearly all samples display a blip in the middle of the plastic deformation region, suggesting that the grippers were not always effective at preventing sample slip.

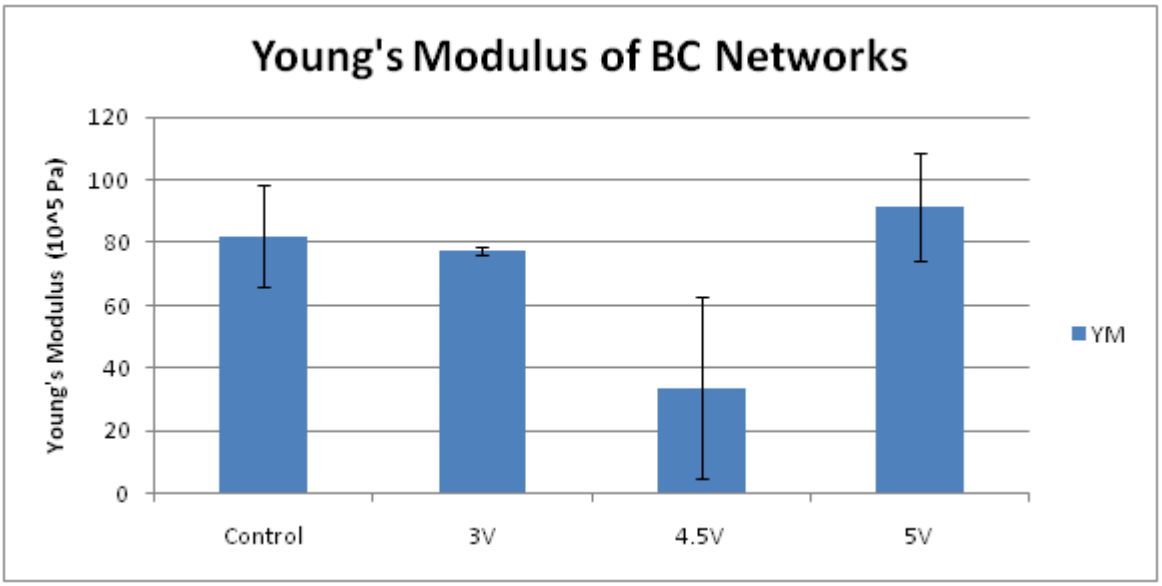

Figure 27: Young's Modulus of samples grown in a 4.5x0.5 cm micro-chamber.

In preliminary experiments, there was no net change in Young's modulus between the control and samples grown under the influence of an electric field. This may be because the material itself has not changed, so its behavior within the elastic (linear) region has not been altered. These values agree with those reported by Bodin et al. [27].

Chapter 4 : **Physical and Chemical Modification**

5.1 Introduction to Physical and Chemical Modification

In the process of completing the experiments outlined in the previous chapters, we noticed that under certain experimental conditions, the nano-structure of the fibers produced had been altered. After further evaluation, it was determined that individual cellulose nano-fibers had become encased in a layer of ions. We hypothesize that the dielectric cellulose fibers become polarized creating regions of positive charge, neutral charge, and negative charge along the fiber (Figure 28a). Free ions within the solution are attracted to regions of charge through electrochemical forces. In the case of a copper rich solution, copper+ ions are attracted to the negative regions of the fibers (Figure 28b). A molecular bond forms at these locations and a crystallization seeding site is initiated. Regions which have been coated by conductive ions are no longer dielectric and the regions of charge distribution progress down the length of the fiber (Figure 28c). This process continues until the length of the fiber (Figure 28d).

Variations in the electrode materials, culture media constituents, and applied field strengths yield a diverse array of cellulose based composites which are bonded at the molecular level. An excess of sodium chloride in combination with aluminum electrodes, for example, was used to create a metal reinforced network in which all of the fibrils were crystallized. The diameter of crystallization is proportional to the process time and applying an electric field for longer durations produces thicker coatings in the fibers. This process has produced copper, aluminum, and titanium nanowires of varying thicknesses.

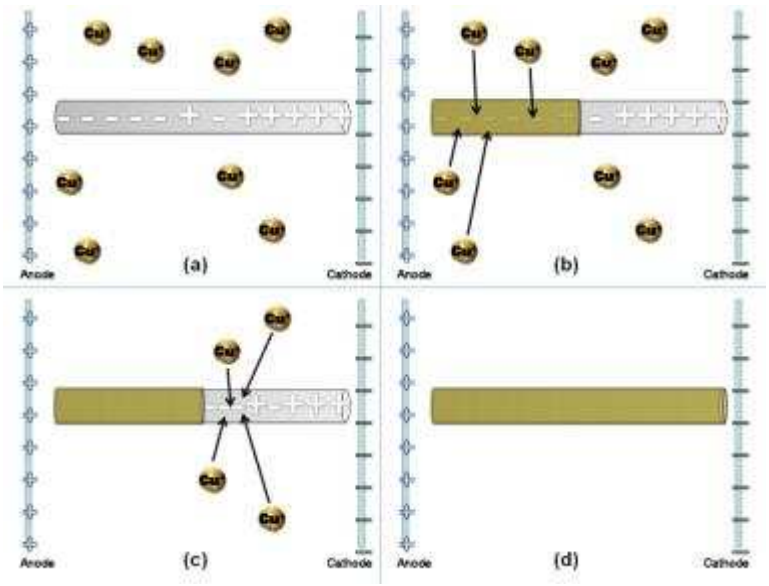

Figure 28: Schematic of the hypothesized process for ion deposition onto a cellulose nano-fiber

This technology has a broad range of applications including the creation of super strong flexible fabrics, electronic circuit fabrication, scaffolds for tissue engineering, and materials for defense and military function. Biofabricated nanotubes may have applications in heat and molecular transport, one dimensional transport, as temperature amplifiers for thermal, electromagnetic, or laser ablation of cancer, or as cages for drug delivery. They can be designed to behave as transistors for nanoscale electronic components.

Biofabricated nanocomposites can be used to make thin sheets for nano-circuit elements and macro-nanoscale interconnects. They can be created with metal reinforcements and calcium crystallizations for durable bone and tissue scaffolds. Their strength and morphology can be directly controlled producing unique materials for textiles, such as bullet proof vests, or military vehicle body armor. This phenomenon has not been extensively investigated and will remain the subject of future work; however, a brief outline of current results is presented below.

5.2 Methods of Physical and Chemical Modification

Acetobacter xylinum cells were cultured as described previously. Precautions were taken to minimize risk of contamination of the bacterial cultures. These included isolating all cultures from immediate contact with general lab equipment by incubating them in an oven (at 30C) housed within a chemical fume hood. All surfaces within the hood were regularly cleaned with ethanol; objects and material were cleaned with ethanol before being placed within the hood or the oven. Additionally, it was required that gloves be worn at all times when handling samples or devices to limit the cultures exposure to external agents. Though *A. xylinum* is non-pathogenic, the bacterium was treated in a similar manner to

materials prescribing to Bio-Safety-Level 2. This resulted in continuous cultures which yielded large densities of cells that could be utilized for weeks.

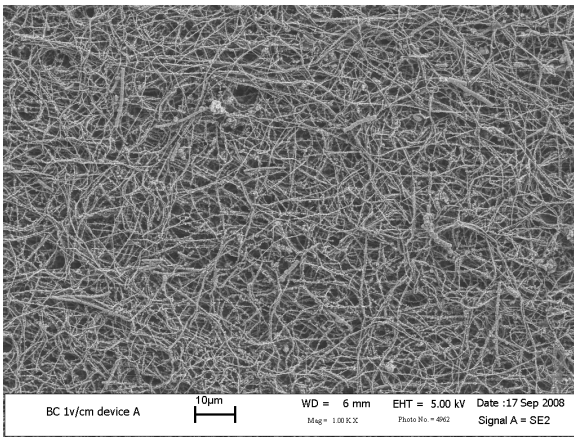

Figure 29: Copper coated cellulose network produced under the influence of a 1V/cm (1.5V) electric field.

The bacteria could be cultured under an electric field in a number of vessels including microfluidic channels, micro-growth chambers, test tubes, and beakers resulting in ion-coated cellulose nano-fibers. In all cases it was necessary to ensure that the electrodes remain in contact with the culture media for the entire duration of the experiment. The ions deposited onto the cellulose network were generally reduced from the electrodes. This coupled with the prolonged duration of the experiments (up to 7 days) occasionally resulted in the complete deterioration of thin electrodes (22 gauge and higher).

5.3 Interesting Results

a. Copper Nanowires

This phenomenon was first discovered when a copper wire was used as an electrode in a micro-growth experiment in which 1V/cm (1.5V) was applied for 48 hours. The experiment failed to produce a significant quantity of cellulose near the electrodes and the cellulose produced had a green hue to it. The network was not a solid structure and could be easily smeared. Imaging of the sample using FESEM revealed a network of copper ion chains. Closer examination revealed that there exists a single cellulose nano-fiber inside each chain.

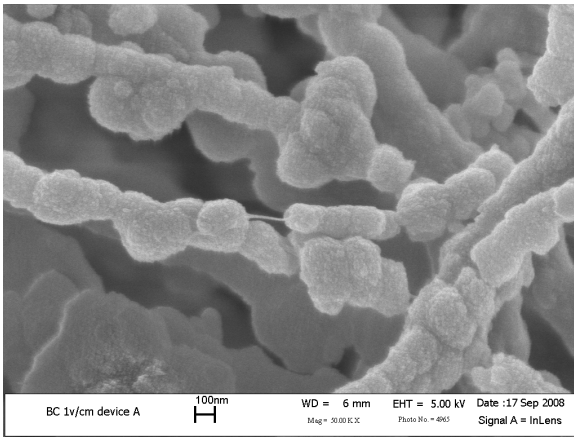

Figure 30: An individual cellulose fiber surrounded by copper ions forming an interconnected network.

The insignificant quantity of cellulose produced near the electrodes can be explained by the cyto-toxicity of copper. Because of this, there are a number of challenges which must be over come in the production of copper-cellulose wires. The concentration of bacterial cells should be extraordinarily high so that production of cellulose can be extended. This may require centrifuging inoculated cells from a large volume (10 -100mL) and suspending them in a small experimental volume (100-500 μL).

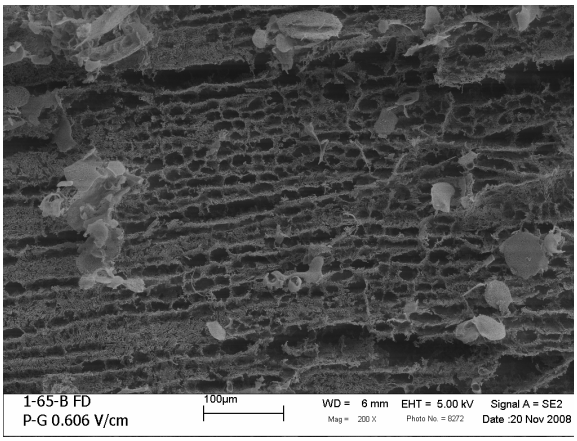

Figure 31: A cellulose-carbon composite created by applying an electric field of 0.606V/cm (1V) using graphite electrodes.

b. *Graphite Composite*

Any conducting material can be used as an electrode in these experiments and in attempting to explore this phenomenon copper, graphite, aluminum, and platinum electrodes were used. The graphite electrodes yielded the most interesting results. It appears that under an applied field of 0.606V/cm (1V) carbon has deposited onto the cellulose fibers. There is a semi-organized structure, but no clear pattern can be determined due to the extensive crystallization. In contrast to the material produced with copper electrodes, the micro-growth chamber was completely filled with cellulose and the network could be removed and handled easily.

c. *Platinum Coatings*

In general, platinum is an inert material and is often used in microfluidic experiments due to its low electrode-fluid interaction. Surprisingly, platinum deposition was observed at electric fields as low as 0.15V/cm (0.25V) after 48 hours of culture. Similar

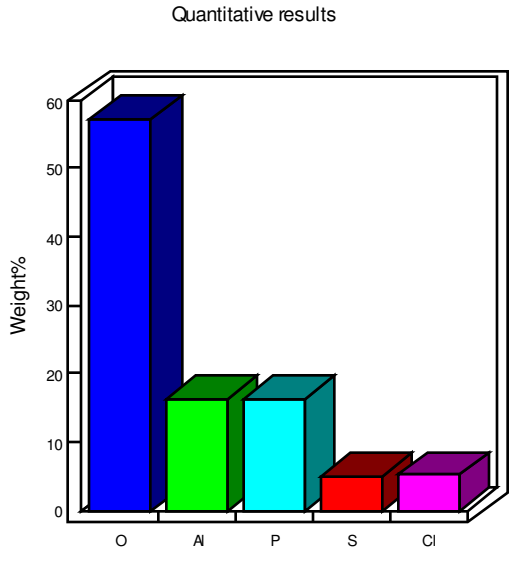

Figure 33: Elemental detection results for the cellulose network produced in a 25% PBS culture media under the application of 0.44V/cm (2V) by aluminum electrodes shows an increased presence of phosphorous and aluminum.

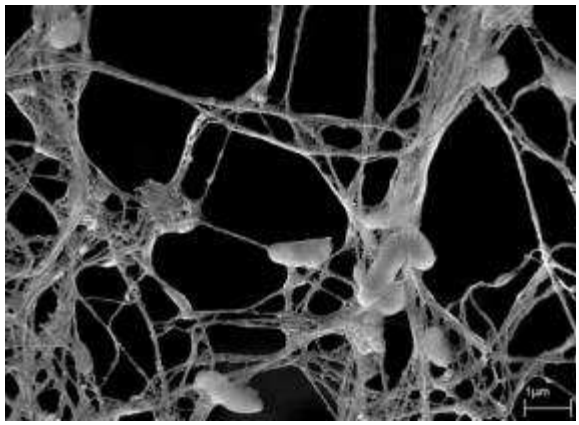

Figure 32: Platinum deposited onto a cellulose network cultured under the influence of a 0.15V/cm (0.25V) electric field.

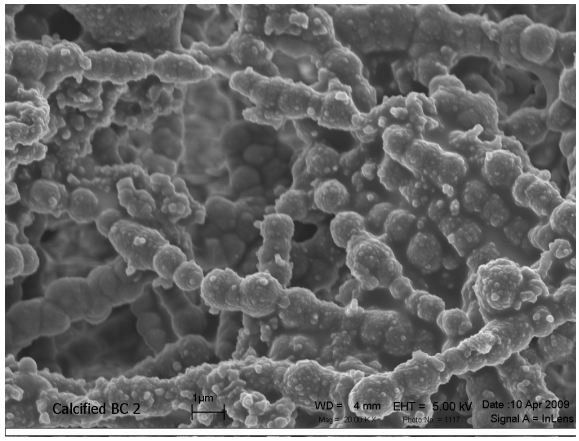

Figure 34: Phosphorous deposited onto a cellulose network cultured under the influence of a 0.44V/cm (2.0V) electric field.

results were observed at higher electric field intensities. Imaging of this network with FESEM was easier than non-coated cellulose. Typically, to achieve a high level of resolution, a relatively thin 5 nanometer layer of gold is deposited onto samples prior to imaging. Exposure to the electron beam often distorts these networks after a few seconds of exposure. The platinum coated networks did not deform as readily suggesting a significant quantity of platinum had been deposited onto the cellulose.

d. *Phosphate Crystallization*

We hypothesize that this phenomenon is a result of

free ions within the solution depositing onto the cellulose network. To validate this, an excess of phosphorous ions were added to the culture media by mixing phosphate buffer solution to the standard H-S culture media in a ratio of 1:4. Cellulose growth within this modified media was evaluated and was found not to change significantly. 100μL of the modified culture media was added to micro-growth chambers (4.5cm x 0.5cm x 500μm). Aluminum electrodes were used to apply a 0.44 V/cm (2.0V) electric field for 96 hours. FESEM imaging revealed a network of cellulose fibers completely surrounded by phosphorous. Elemental detection reviled nearly 100% increase by weight of phosphorous as compared to control samples.

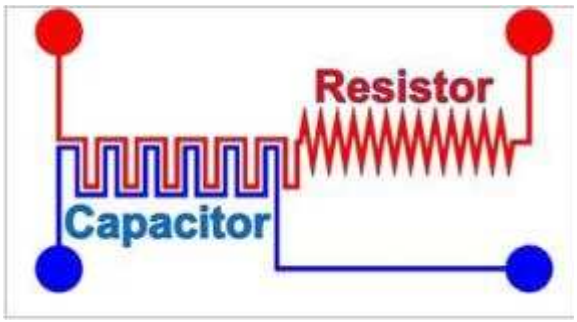

Figure 35: Schematic of the resistor-capacitor microfluidic channel pair.

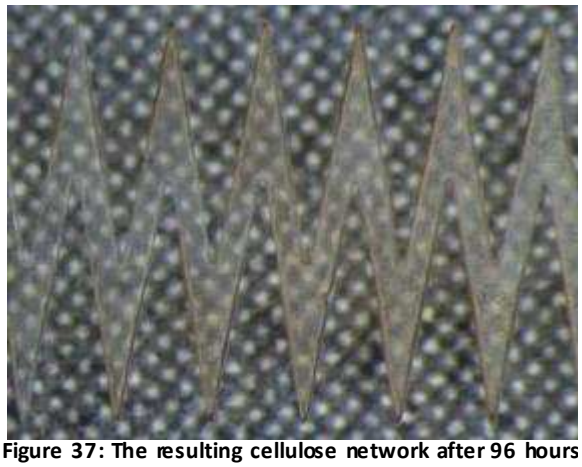

Figure 37: The resulting cellulose network after 96 hours of cultivation under 0.152V/cm (1.35V) applied by aluminum electrodes.

conductive bacterial cellulose

A Silicon master stamp fabricated via standard photolithography and Deep Reactive Ion Etching was used to create microfluidic channel pairs in PDMS. These channels were specifically designed such that the resultant circuit, after conductive cellulose cultivation, will behave as a passive low pass filter. The bacteria were introduced into the inlet ports of the channels. Electrodes were then inserted into the inlet ports and activated. Future experimentation should focus A cellulose network was successfully grown in the microfluidic channel pair with electric fields of 0.152V/cm (1.35V) and 0.281V/cm (1.35V) in

e. Resistor-Capacitor Circuit

Preliminary experiments yielded a bulk material which was transparent, making this an ideal material for applications such as electronic paper and textile electronics. The objective of these experiments will be to develop a passive signal attenuation circuit of

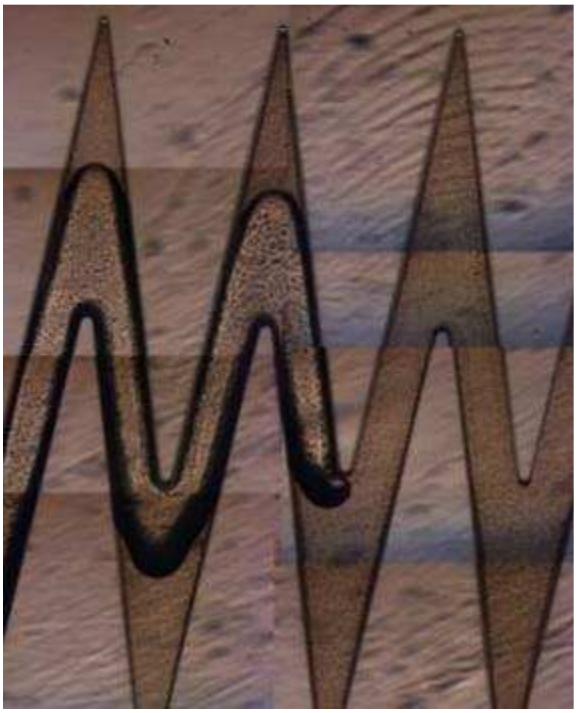

Figure 36: Composite image of the resistive leg after 48 hours of cultivation showing the progression of metallization through the channel.

the resistive and capacitive legs respectively. The network imaged using light microscopy during cultivation and after being removed from the microfluidic channels. Future work will focus on FESEM imaging, measuring of the resistive, capacitive, and inductive properties of the circuit, phase and spectral response of the entire circuit and evaluation of the Cutoff frequency (-3dB point), signal to noise ratio, and roll off order.

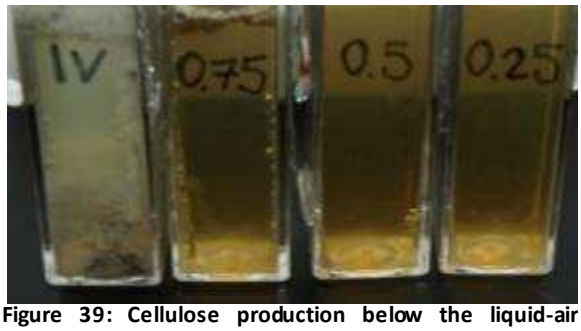

Figure 39: Cellulose production below the liquid-air interface observed when the applied voltage reaches 1.0V

The electric field was removed every 24 hours while the sample was being imaged. A region of 'metalized' cellulose could be seen progressing through the channel over 72 hours.

f. Sub-surface Cellulose Production

A brief experiment was run to analyze the effect of cellulose production below the liquid-air interface under the application of an electric field. Four 1cm square plastic cuvettes were modified by applying a conductive aluminum tape along two opposing internal edges. This provided electrodes which were used to apply an electric field within the culture media. The cuvettes were filled to 75% capacity and electric fields of 0.25, 0.5, 0.75 and 1V/cm were applied for 48 hours. Cellulose production at the liquid-air interface was observed for all experimental parameters. Cellulose production below the liquid-air boundary was only observed in the 1V/cm cuvette and is likely the result of oxygen production due to electrolysis.

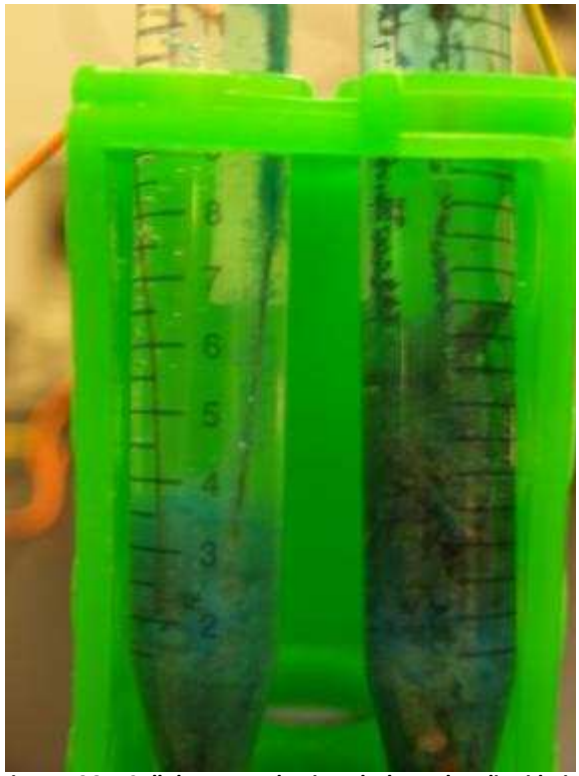

Figure 38: Cellulose production below the liquid-air interface after 8 hours under the application of 16V in test tubes containing tap water (left) and tap water with methylene blue(right).

Similar experiments were conducted in test tubes containing 12mL of tap water and 100μL of inoculated culture media. After 30 minutes, cellulose could be seen in the fluid and rising to the top of the test tube. Some cellulose near the electrodes appeared to be turning a light blue color. The current flowing through the system decreased from 0.125A to 0.086A from the onset to 30 minutes respectively. After 8 hours there was minimal increase in the observed quantity of cellulose produced suggesting that the level of copper ions within the solution had reached a cytotoxic level and the electrodes had almost completely disintegrated.

The experiment was repeated with the addition of a small quantity of methylene blue to the fluid. After 8 hours, the test tube was almost completely clear with deep blue sediment at the bottom of the test tube. It appears that the application of an electric field during the cultivation process allows for the cellulose to bind with other molecules in the solution.

Chapter 5 : **Future Work**

Though an extensive effort has been made to understand the effects of an electro-magnetic field on the biofabrication of cellulose nanofibers, there remain a number of studies that must be completed to fully understand this phenomenon.

6.1 Comprehensive Examination on the Effects of Electric Field Intensity

The results presented herein may not clearly define the whole regime in which an electric field alters the morphology of the cellulose network produced. This is a result of the narrow theoretical range in which the electric field will change the morphology without impeding cellulose production and the challenges associated with accurately producing an electric field within this region. For example a 1V signal applied to a 1cm long micro-growth chamber would theoretically result in a 1V/cm electric field. However, the manufacturing processes for creating these devices require inlet ports to be punched by hand and wires to be inserted into reservoirs. In individual devices, the inlet ports may be inaccurately punched and the wires may not be inserted to a distance of exactly 1cm from one another. Consider a hypothetical situation in which two identical devices have electrode separation distances of 1cm in device 1 and 0.8 cm in device two. This will result in a 20% difference in electric field intensity between the two devices. When considering that there is a vast difference in the cellulose network produced under 0.33V/cm and that produced und 0.45V/cm (a 26% increase), errors in experimental tolerance could be disastrous. The results presented previously were conducted under experimental conditions which rigorously attempted to minimize such errors. To fully understand this phenomenon, future studies should focus on electric field strengths between 0.15V/cm and 0.75V/cm increasing by 0.05V/cm in micro-growth chambers.

Electrokinetics and dielectrophoresis are microfluidic phenomenon. Significant work will need to be done to examine the limits in dimension in which these forces will continue to dominate the microbial motion.

6.2 Comprehensive Mechanical Testing

A preliminary study was completed on the cellulose networks produced under an electric field. These demonstrated that the electric field produces cellulose networks with a longer elongation to break than control networks, but no significant change in Young's modulus. Based on these results it is clearly necessary to run a more rigorous set of experiments on cellulose networks produced in the presence of electric fields between 0.1 and 1V/cm. Since *A. xylinum* shut off cellulose production when they are

agitated too much, there should exist a region in which the interconnected network of cellulose becomes less entangled resulting in a weaker structure. Likewise a network of aligned fibers should no longer display the anisotropy of native networks and tensile testing of the networks in the direction perpendicular to the electric field should be conducted.

6.3 Alternating Signals and Complex Network Morphologies

For these networks to be useful in a physiological sense, the network structure must be more complex than simple alignment of fibers. Many physiological tissues, such as the meniscus, have complex fiber orientations in which the fibers are oriented in radial and cross-hatched patterns. To produce cellulose networks with these morphologies a combination of switched DC and AC fields will need to be used.

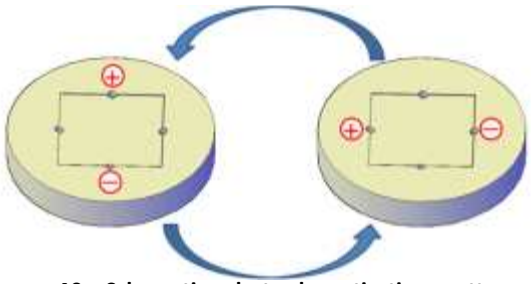

Figure 40: Schematic electrode activation pattern to produce zig-zag patterned nano-cellulose

While mimicking physiological orientations is an important step in developing this technology, it is fundamentally important and theoretically possible to create materials with completely different mechanical properties. This technology makes it possible to alter the nano-structure of a material as it is being fabricated. With this, it is possible to create a closed cell network which results in a material with a negative modulus (Auxetic or anti-rubber).

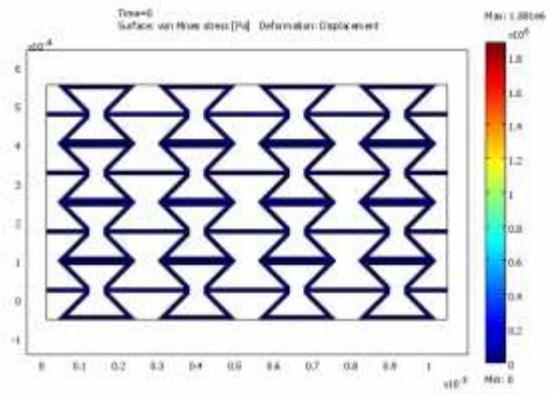

Figure 41: Schematic of a nano-structure which will result in a negative Young's modulus. A material with this structure will expand in all directions when pulled in one direction.

Chapter 6 : **Conclusion**

Control of the 3D morphology of cellulose networks from the nanoscale to the macroscale is a critical aspect in developing customizable implants and scaffolds for tissue engineering, since the biological responses of cells in these materials is strongly correlated to the nanoscale topography[61]. We have demonstrated that this can be attained by controlling the movement of *A. xylinum* at the nanoscale by electric fields to create custom cellulose networks. The results of this study demonstrate the first direct control over a bottom up biofabrication process in three dimensions. By carefully controlling the electrokinetic forces, we can navigate the bacteria while they extrude cellulose networks. The manipulation of electrokinetic forces acting upon a bacterial cell can produce complex cellulose patterns on the nanoscale not achievable in static culture.

This offers, in addition to control of the material architecture, benefits from an environmental point of view. Our biofabrication process uses sugar and nutrients which can come from directly agricultural waste streams. Also, we operate at room temperature and use weak electric fields. Furthermore, we do not use chemicals and the materials produced are biodegradable.

The ability to control the direction of fiber orientation could be readily expanded to weave structures of multiple fiber layers, with each layer grown in a prescribed direction, by simply changing the orientation of the applied electric field, and these structures could be tailored to have the desired mechanical properties for a variety of applications including tissue engineering, MEMS, textiles, and electronics. Future work will focus on evaluating the mechanical properties of scaffolds with aligned fibers and creating scaffolds with complex fiber orientations suitable for biomedical implants. We are convinced that *A. xylinum* is not the only example of a biological system which can be controlled and the combination of multiple biological agents could be used to produce distinctive materials, connected at the nanoscale, which are morphologically and mechanically different from existing materials.

Chapter 7 : **References**

1. A. Hirai, and F. Horii, "Cellulose assemblies produced by Acetobacter xylinum," ICR Annual Report **6,** 28-29 (2000).
2. L. Q. Wu, and G. F. Payne, "Biofabrication: using biological materials and biocatalysts to construct nanostructured assemblies," Trends in Biotechnology **22,** 593-599 (2004).
3. M. H. Zareie, H. Ma, B. W. Reed, A. K. Y. Jen, and M. Sarikaya, "Controlled assembly of conducting monomers for molecular electronics," Nano Letters **3,** 139-142 (2003), <Go to ISI>://000181001500007.
4. H. Zhou, T. X. Fan, T. Han, X. F. Li, J. Ding, D. Zhang, Q. X. Guo, and H. Ogawa, "Bacteria-based controlled assembly of metal chalcogenide hollow nanostructures with enhanced light-harvesting and photocatalytic properties," Nanotechnology **20,** (2009), <Go to ISI>://000263071100015.
5. S. W. Lee, C. B. Mao, C. E. Flynn, and A. M. Belcher, "Ordering of quantum dots using genetically engineered viruses," Science **296,** 892-895 (2002), <Go to ISI>://000175442500039.
6. R. V. Davalos, G. J. McGraw, T. I. Wallow, A. M. Morales, K. L. Krafcik, Y. Fintschenko, E. B. Cummings, and B. A. Simmons, "Performance impact of dynamic surface coatings on polymeric insulator-based dielectrophoretic particle separators," Anal. Bioanal. Chem. **390,** 847-855 (2008).
7. H. A. Pohl, "The Motion and Precipitation of Suspensoids in Divergent Electric Fields," Journal of Applied Physics **22,** 869-871 (1951), http://dx.doi.org/10.1063/1.1700065.
8. P. R. C. Gascoyne, J. V. Vykoukal, J. A. Schwartz, T. J. Anderson, D. M. Vykoukal, K. W. Current, C. McConaghy, F. F. Becker, and C. Andrews, "Dielectrophoresis-based programmable fluidic processors," Lab on a Chip **4,** 299-309 (2004).
9. J. El-Ali, P. K. Sorger, and K. F. Jensen, "Cells on chips," Nature **442,** 403-411 (2006), http://dx.doi.org/10.1038/nature05063.
10. B. A. Simmons, G. J. McGraw, R. V. Davalos, G. J. Fiechtner, Y. Fintschenko, and E. B. Cummings, "The development of polymeric devices as dielectrophoretic separators and concentrators," MRS Bulletin **31,** 120-124 (2006).
11. H. Shafiee, J. L. Caldwell, M. B. Sano, and R. V. Davalos, "Contactless dielectrophoresis: a new technique for cell manipulation," Biomedical Microdevices **11,** 997-1006 (2009).
12. J. C. Giddings, and S. L. Brantley, "SHEAR FIELD-FLOW FRACTIONATION - THEORETICAL BASIS OF A NEW, HIGHLY SELECTIVE TECHNIQUE," Sep. Sci. Technol. **19,** 631-651 (1984).
13. C. B. Fuh, "Split-flow thin fractionation," Anal. Chem. **72,** 266A-271A (2000).
14. C. B. Fuh, and S. Y. Chen, "Magnetic split-flow thin fractionation of magnetically susceptible particles," J. Chromatogr. A **857,** 193-204 (1999).
15. T. M. Vickrey, and J. A. Garciaramirez, "MAGNETIC FIELD-FLOW FRACTIONATION - THEORETICAL BASIS," Sep. Sci. Technol. **15,** 1297-1304 (1980).
16. A. Kolin, "An Electromagnetokinetic Phenomenon Involving Migration of Neutral Particles," Science **117,** 134-137 (1953).
17. A. Kolin, and R. T. Kado, "Fractionation of Cell Suspensions in an Electromagnetic Force Field," Nature **182,** 510-512 (1958).
18. R. M. Nalbandian, R. E. Michel, and I. Mader, "Paramagnetism of human serum proteins demonstrated by two-stage electromagnetophoresis," Cellular and Molecular Life Sciences **24,** 1006-1007 (1968).

19. L. Cellini, R. Grande, E. Di Campli, S. Di Bartolomeo, M. Di Giulio, I. Robuffo, O. Trubiani, and M. A. Mariggio, "Bacterial response to the exposure of 50 Hz electromagnetic fields," Bioelectromagnetics **29,** 302-311 (2008).
20. L. Fojt, P. Klapetek, L. Strasak, and V. Vetterl, "50 Hz magnetic field effect on the morphology of bacteria," Micron **40,** 918-922 (2009), <Go to ISI>://000270264700023.
21. R. M. Brown, J. H. M. Willison, and C. L. Richardson, "Cellulose Biosynthesis In Acetobacter-Xylinum - Visualization Of Site Of Synthesis And Direct Measurement Of Invivo Process.," Proc. Natl. Acad. Sci. U. S. A. **73,** 4565-4569 (1976).
22. R. M. Brown, C. Haigler, and K. Cooper, "EXPERIMENTAL INDUCTION OF ALTERED NON-MICROFIBRILLAR CELLULOSE," Science **218,** 1141-1142 (1982).
23. H. Backdahl, G. Helenius, A. Bodin, U. Nannmark, B. R. Johansson, B. Risberg, and P. Gatenholm, "Mechanical properties of bacterial cellulose and interactions with smooth muscle cells," Biomaterials **27,** 2141-2149 (2006).
24. G. Helenius, H. Backdahl, A. Bodin, U. Nannmark, P. Gatenholm, and B. Risberg, "In vivo biocompatibility of bacterial cellulose," Journal of Biomedical Materials Research Part A **76A,** 431-438 (2006).
25. D. Klemm, D. Schumann, U. Udhardt, and S. Marsch, "Bacterial synthesized cellulose - artificial blood vessels for microsurgery," Progress in Polymer Science **26,** 1561-1603 (2001).
26. A. Svensson, E. Nicklasson, T. Harrah, B. Panilaitis, D. L. Kaplan, M. Brittberg, and P. Gatenholm, "Bacterial cellulose as a potential scaffold for tissue engineering of cartilage," Biomaterials **26,** 419-431 (2005).
27. A. Bodin, S. Concaro, M. Brittberg, and P. Gatenholm, "Bacterial cellulose as a potential meniscus implant," Journal of Tissue Engineering and Regenerative Medicine **1,** 406-408 (2007).
28. A. Bodin, H. Backdahl, H. Fink, L. Gustafsson, B. Risberg, and P. Gatenholm, "Influence of cultivation conditions on mechanical and morphological properties of bacterial cellulose tubes," Biotechnology and Bioengineering **97,** 425-434 (2007).
29. A. Putra, A. Kakugo, H. Furukawa, J. P. Gong, Y. Osada, T. Uemura, and M. Yamamoto, "Production of bacterial cellulose with well oriented fibril on PDMS substrate," Polymer Journal **40,** 137-142 (2008).
30. A. Putra, A. Kakugo, H. Furukawa, J. P. Gong, and Y. Osada, "Tubular bacterial cellulose gel with oriented fibrils on the curved surface," Polymer **49,** 1885-1891 (2008).
31. Y. Uraki, J. Nemoto, H. Otsuka, Y. Tamai, J. Sugiyama, T. Kishimoto, M. Ubukata, H. Yabu, M. Tanaka, and M. Shimomura, "Honeycomb-like architecture produced by living bacteria, Gluconacetobacter xylinus," Carbohydrate Polymers **69,** 1-6 (2007).
32. T. Kondo, M. Nojiri, Y. Hishikawa, E. Togawa, D. Romanovicz, and R. M. Brown, "Biodirected epitaxial nanodeposition of polymers on oriented macromolecular templates," Proc. Natl. Acad. Sci. U. S. A. **99,** 14008-14013 (2002).
33. D. P. J. Barz, and P. Ehrhard, "Model and verification of electrokinetic flow and transport in a micro-electrophoresis device," Lab on a Chip **5,** 949-958 (2005).
34. V. Tandon, S. K. Bhagavatula, W. C. Nelson, and B. J. Kirby, "zeta potential and electroosmotic mobility in microfluidic devices fabricated from hydrophobic polymers: 1. The origins of charge," Electrophoresis **29,** 1092-1101 (2008).
35. Y. J. Kang, and D. Q. Li, "Electrokinetic motion of particles and cells in microchannels," Microfluidics and Nanofluidics **6,** 431-460 (2009).
36. H. A. Pohl, "Some Effects of Nonuniform Fields on Dielectrics," Journal of Applied Physics **29,** 1182-1188 (1958), http://dx.doi.org/10.1063/1.1723398.
37. A. Atala, "Experimental and clinical experience with tissue engineering techniques for urethral reconstruction," Urologic Clinics of North America **29,** 485-+ (2002), <Go to ISI>://000178226000022.

38. R. E. De Filippo, J. J. Yoo, and A. Atala, "Urethral replacement using cell seeded tubularized collagen matrices," in *Annual Meeting of the Section-on-Urology-American-Academy-of-Pediatrics*, (San Francisco, California, 2001), pp. 1789-1792.
39. A. A. Caldamone, and D. A. Diamond, "Long-term results of the endoscopic correction of vesicoureteral reflux in children using autologous chondrocytes," in *Joint Meeting of the American-Academy-of-Pediatrics Section on Urology/European-Society-for-Paediatric-Urology*, (Tours, France, 2000), pp. 2224-2227.
40. J. S. Temenoff, and A. G. Mikos, "Review: tissue engineering for regeneration of articular cartilage," Biomaterials **21,** 431-440 (2000).
41. Y. S. Nam, J. J. Yoon, and T. G. Park, "A novel fabrication method of macroporous biodegradable polymer scaffolds using gas foaming salt as a porogen additive," Journal of Biomedical Materials Research **53,** 1-7 (2000).
42. H. Lo, M. Ponticiello, and K. W. Leong, "Fabrication of controlled release biodegradable foams by phase separation," Tissue Engineering**,** 15-28 (1995).
43. Q. L. Zhou, Y. H. Gong, and C. Y. Gao, "Microstructure and mechanical properties of poly(L-lactide) scaffolds fabricated by gelatin particle leaching method," Journal of Applied Polymer Science **98,** 1373-1379 (2005), <Go to ISI>://000231830500059.
44. J. Stitzel, L. Liu, S. J. Lee, M. Komura, J. Berry, S. Soker, G. Lim, M. Van Dyke, R. Czerw, J. J. Yoo, and A. Atala, "Controlled fabrication of a biological vascular substitute," Biomaterials **27,** 1088-1094 (2006), <Go to ISI>://000234148300017.
45. B. S. Harrison, D. Eberli, S. J. Lee, A. Atala, and J. J. Yoo, "Oxygen producing biomaterials for tissue regeneration," Biomaterials **28,** 4628-4634 (2007), <Go to ISI>://000249717500010.
46. S. F. Yang, K. F. Leong, Z. H. Du, and C. K. Chua, "The design of scaffolds for use in tissue engineering. Part 1. Traditional factors," Tissue Engineering **7,** 679-689 (2001).
47. L. G. Griffith, and G. Naughton, "Tissue engineering - Current challenges and expanding opportunities," Science **295,** 1009-+ (2002).
48. H. J. Son, H. G. Kim, K. K. Kim, H. S. Kim, Y. G. Kim, and S. J. Lee, "Increased production of bacterial cellulose by Acetobacter sp V6 in synthetic media under shaking culture conditions," Bioresource Technology **86,** 215-219 (2003).
49. K. A. Zimmermann, J. M. L. J.M., S. K.T., R. W. Fox, and P. Gatenholm, "Biomimetic design of a bacterial cellulose/hydroxyapatite nanocomposite for bone healing applications," Mater. Sci. Eng. C**,** (2009).
50. C. S. Szot, C. F. Buchanan, P. Gatenholm, M. N. Rylander, and J. W. Freeman, "Investigation of cancer cell behavior on nanofibrous scaffolds," Mater. Sci. Eng. C**,** (2009).
51. G. Wang, X. F. Chen, X. D. Shi, L. J. Yu, B. F. Liu, and G. Yang, "Bio-fabrication of patterned cellulose nano-fibers," in *International Conference on Multifunctional Materials and Structures*, A. K. T. L. J. V. V. K. C. F. K. T. J. P. L. P. M. Lau, ed. (Hong Kong, PEOPLES R CHINA, 2008), pp. 1359-1362.
52. W. Czaja, D. Romanovicz, and R. M. Brown, "Structural investigations of microbial cellulose produced in stationary and agitated culture," Cellulose **11,** 403-411 (2004).
53. S. Archer, T. T. Li, A. T. Evans, S. T. Britland, and H. Morgan, "Cell reactions to dielectrophoretic manipulation," Biochem. Biophys. Res. Commun. **257,** 687-698 (1999).
54. H. Berg, "POSSIBILITIES AND PROBLEMS OF LOW-FREQUENCY WEAK ELECTROMAGNETIC-FIELDS IN CELL BIOLOGY," Bioelectrochem. Bioenerg. **38,** 153-159 (1995).
55. R. Huang, L. Peng, and L. Hertz, "Effects of a low-voltage static electric field on energy metabolism in astrocytes," Bioelectromagnetics **18,** 77-80 (1997).
56. W. J. Ji, H. M. Huang, A. H. Deng, and C. Y. Pan, "Effects of static magnetic fields on Escherichia coli," Micron **40,** 894-898 (2009).

57. A. Krystynowicz, W. Czaja, A. Wiktorowska-Jezierska, M. Goncalves-Miskiewicz, M. Turkiewicz, and S. Bielecki, "Factors affecting the yield and properties of bacterial cellulose," Journal of Industrial Microbiology & Biotechnology **29,** 189-195 (2002).
58. P. G. Verschuren, T. D. Cardona, M. J. R. Nout, K. D. De Gooijer, and J. C. Van den Heuvel, "Location and limitation of cellulose production by Acetobacter xylinum established from oxygen profiles," J. Biosci. Bioeng. **89,** 414-419 (2000).
59. D. Dimitrov, H. Isoda, and T. Maekawa, *Proteomic analysis of changes in excitable and non-excitable cells exposed to DC electric fields of physiological strength* (Springer, Dordrecht, 2003).
60. F. Yoshinaga, N. Tonouchi, and K. Watanabe, "Research progress in production of bacterial cellulose by aeration and agitation culture and its application as a new industrial material," Bioscience Biotechnology and Biochemistry **61,** 219-224 (1997).
61. M. M. Stevens, and J. H. George, "Exploring and engineering the cell surface interface," Science **310,** 1135-1138 (2005).